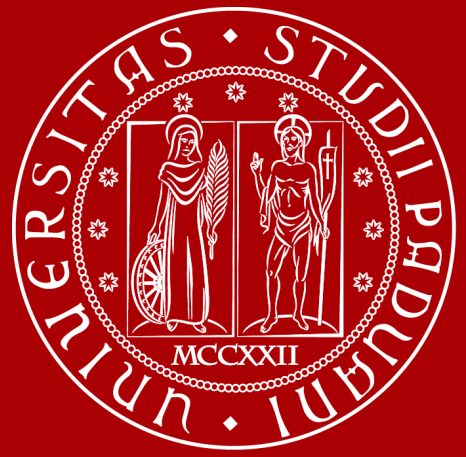

UNIVERSITÀ
DEGLI STUDI
DI PADOVA

Coupled simulation of flow and deformation in fractured porous media: Discretizations, solvers and applications

Massimiliano Ferronato

TU Ostrava, January 27-28, 2025

Seminar of Numerical Analysis ’25 (SNA25) – Winter School

Outline

- **Introduction**
  - *Modeling mechanics and flow in fractured porous media*
- **Mathematical model**
  - *Variational formulation and numerical discretization*
  - *Block algebraic problem and preconditioning*
- **Numerical results**
  - *Validation, stability and convergence*
  - *Solver performance*
  - *Applications*
- **Conclusions and future work**

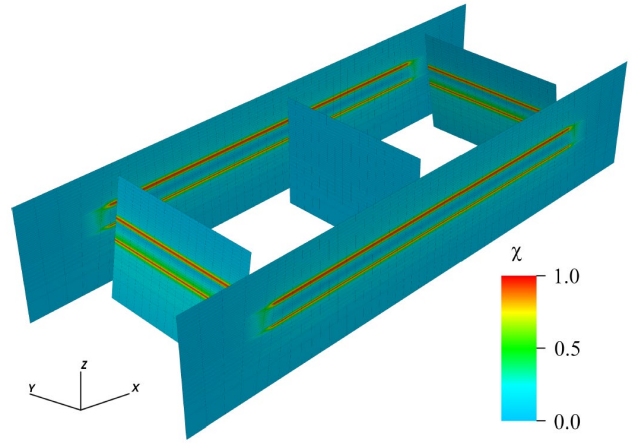

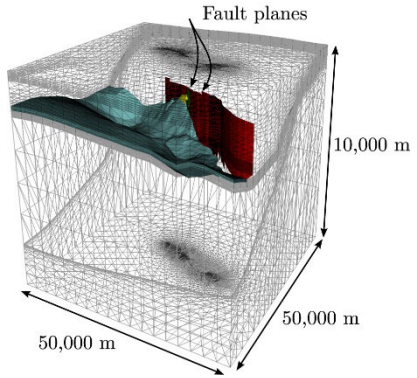

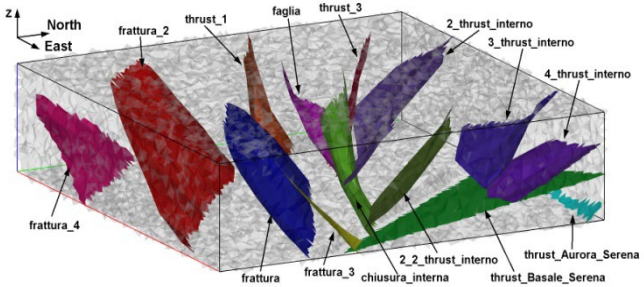

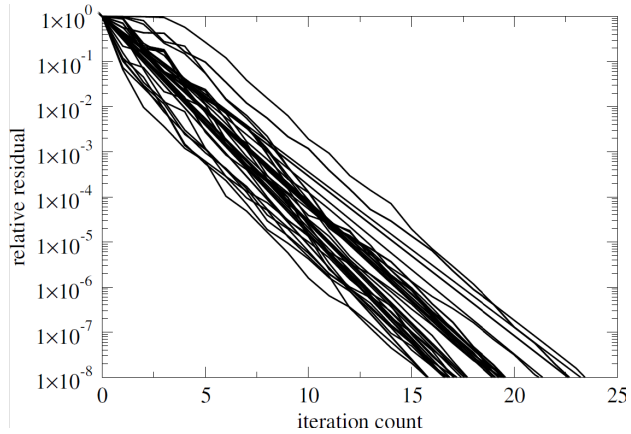

Introduction

Modeling mechanics and flow in fractured media

- ✓ The simulation of flow and mechanics in fractured porous media is of particular interest in many subsurface applications, like geothermal energy production, CO2 sequestration and underground gas storage
- ✓ Faults and fractures are responsible of a number of processes, such as micro-seismic events, fluid leakage or shale-gas production → especially concerned with the **safety** of the subsurface activity
  - Safety of underground storage of wastes and hydrocarbon
  - Ground ruptures due to water withdrawal in arid regions
  - Triggered or induced seismicity

- ✓ A fault is a deteriorated portion of rock characterized by:
  - the core filled with fine-grained and impermeable material derived from the gradual fracturing of the grains (cataclasis)
  - an inner damage zone with a high density of micro-fractures (rock joints) that can generate and propagate
  - an outer damage zone with a deformation bands giving rise to subsidiary faults

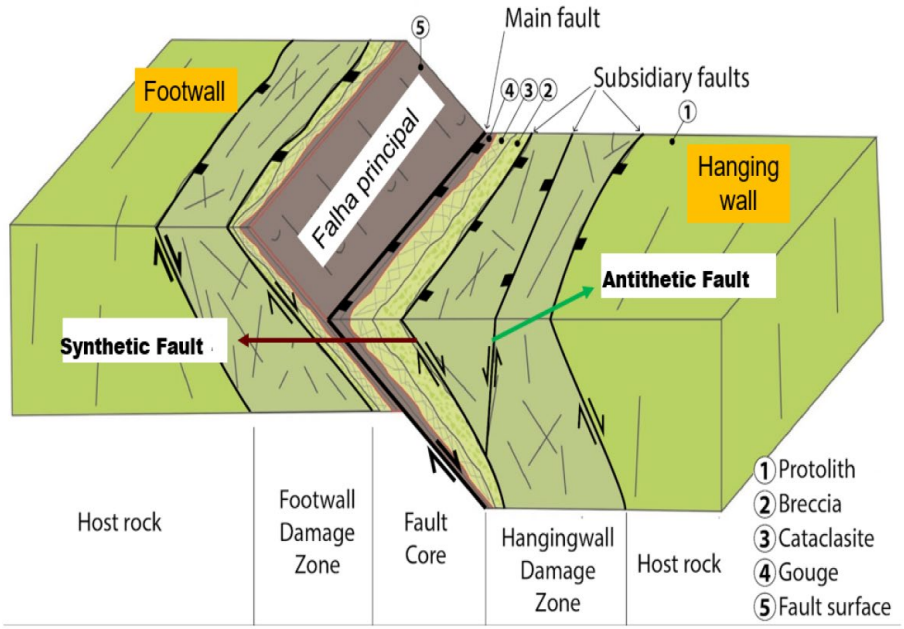

- ✓ Permeability in a fault is strongly anisotropic → k_N increases towards the core, then abruptly goes to zero
  → k_T abruptly increases in the core at the fault activation
- ✓ Though it is a 3D region, the plain size is much larger than the normal size, so that it is often approximated by a lower-dimensional entity

Introduction

Modeling mechanics and flow in fractured media

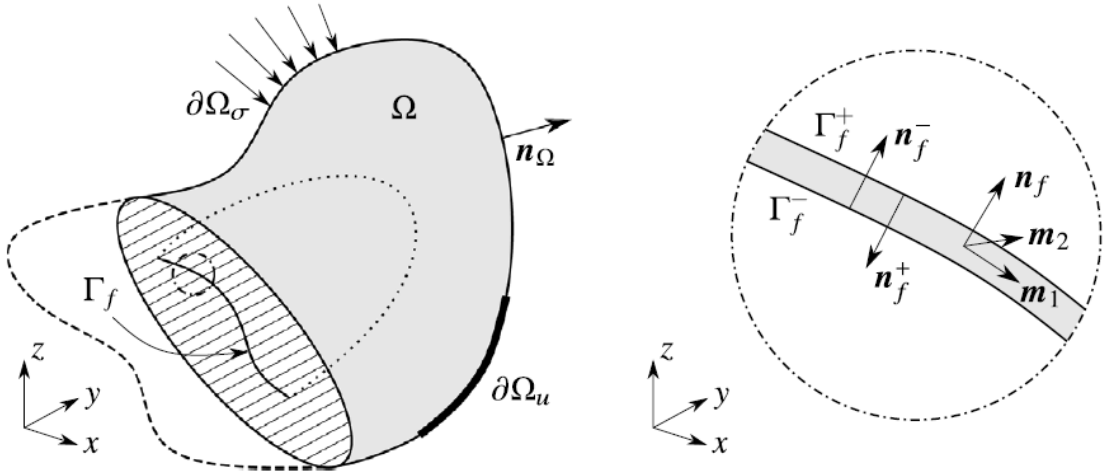

- ✓ A fault can be modelled as a discontinuity within a 3D porous body made of a pair of friction surfaces in contact each other
- ✓ The surfaces can't penetrate, and continuity is preserved if $\tau < \tau_L = c - \sigma_n \tan\varphi$ (Mohr-Coulomb criterion)
- ✓ Traction on the fault is the quantity controlling the activation

- ✓ The Mohr-Coulomb criterion defines τ_L, but gives no indication as to the direction of the limiting shear vector $\boldsymbol{t}_L$
- ✓ According to the Principle of Maximum Plastic Dissipation, $\boldsymbol{t}_L$ is such that the friction work $\mathcal{W}_f$ is maximum, i.e., it is parallel to the slip vector $\boldsymbol{u}_r$:

$$\boldsymbol{t}_L = \tau_L \frac{\boldsymbol{u}_r}{\|\boldsymbol{u}_r\|_2}$$

✓ Modeling the mechanics of fractures in porous media involves several numerical issues, which are still largely unresolved:

1. **Continuous Finite Elements** with a different rheology [Rutqvist et al. 2008]
   - Pros → Ease of implementation
   - Cons → Inability to describe slippage and opening
2. **Interface frictional elements** by penalties [Beer, 1985; Cescotto & Charlier, 1993; Juanes et al., 2002; Ferronato et al., 2008]
   - Pros → Definiteness preservation, controlled number of DoFs
   - Cons → Ill-conditioning, instability, non-linear convergence difficulties
3. **Lagrange multipliers** [Aagaard et al., 2013; Jha & Juanes, 2014; Franceschini et al., 2016; 2020]
   - Pros → Mathematically robust prescription of constraints
   - Cons → Increase of DoFs, saddle-point problem

Mathematical model

Governing PDEs and variational formulation

- Governing PDEs for the linear momentum balance subject to contact constraints:

$$-\nabla \cdot \boldsymbol{\sigma}(\boldsymbol{u}) = \boldsymbol{b} \qquad \forall\, (\boldsymbol{x}, t) \in \Omega \times [0, T] \qquad \text{(equilibrium)}$$

$$t_N = \boldsymbol{t} \cdot \boldsymbol{n}_f \leq 0, \qquad g_N = [\![\boldsymbol{u}]\!] \cdot \boldsymbol{n}_f \geq 0, \qquad t_N g_N = 0 \qquad \forall\, (\boldsymbol{x}, t) \in \Gamma_f \times [0, T] \qquad \text{(impenetrability)}$$

$$\|\boldsymbol{t}_T\|_2 \leq \tau_L = c - t_N \tan\varphi\,, \qquad \boldsymbol{g}_T \cdot \boldsymbol{t}_T = \tau_L \|\boldsymbol{g}_T\|_2 \qquad \forall\, (\boldsymbol{x}, t) \in \Gamma_f \times [0, T] \qquad \text{(friction)}$$

- Let $\boldsymbol{\mathcal{U}} \subset [H^1(\Omega)]^3$ be the first-order Sobolev space of functions in Ω satisfying the essential boundary conditions, with $\boldsymbol{\mathcal{U}}_0$ the related counterpart for homogeneous conditions, and let $\boldsymbol{\mathcal{M}}$ be the dual space of the trace space $\boldsymbol{\mathcal{W}} = \left[H^{1/2}(\Gamma_f)\right]^3$; let us define the subspace $\boldsymbol{\mathcal{M}}(t_N) \subset \boldsymbol{\mathcal{M}}$ such that [Wohlmuth, 2011]:

$$\boldsymbol{\mathcal{M}}(t_N) = \left\{ \boldsymbol{\mu} \in \boldsymbol{\mathcal{M}} : (\boldsymbol{\mu}, \boldsymbol{v})_{\Gamma_f} \leq \tau_L \|\boldsymbol{v}_T\|_2, \boldsymbol{v} \in \boldsymbol{\mathcal{W}} \text{ with } v_N \leq 0 \right\}$$

- Weak variational formulation:

$$(\nabla^s \boldsymbol{\eta}, \boldsymbol{\sigma})_\Omega + ([\![\boldsymbol{\eta}]\!], \boldsymbol{t})_{\Gamma_f} = (\boldsymbol{\eta}, \boldsymbol{b})_{\bar{\Omega}} + (\boldsymbol{\eta}, \bar{\boldsymbol{t}})_{\Gamma_\sigma} \qquad \forall\, \boldsymbol{\eta} \in \boldsymbol{\mathcal{U}}_0 \subset [H^1(\Omega)]^3$$

$$(t_N - \mu_N, g_N)_{\Gamma_f} + (\boldsymbol{t}_T - \boldsymbol{\mu}_T, \boldsymbol{g}_T)_{\Gamma_f} \geq 0 \qquad \forall\, \boldsymbol{\mu} \in \boldsymbol{\mathcal{M}}(t_N)$$

Mathematical model

Discretization and solution algorithm

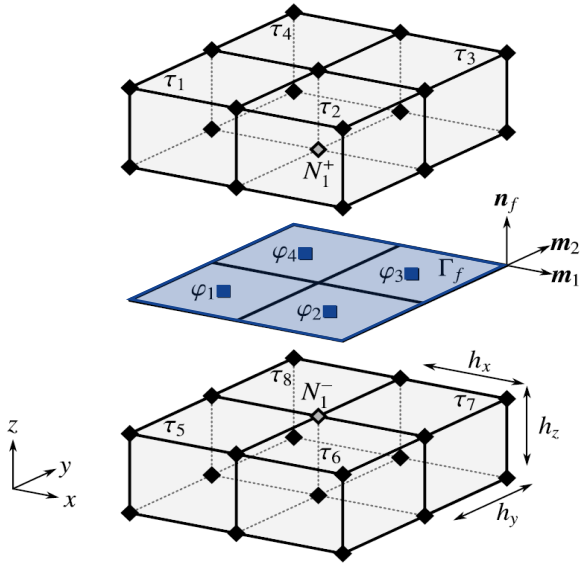

- ✓ We introduce a partitioning of the 3D domain and a conforming discretization of the contact surfaces
- ✓ A typical choice is based on low-order elements: (1) first-order continuous finite elements for displacement unknowns; (2) face-centered piecewise-constant finite elements for traction
- ✓ This choice is usually consistent with the Finite Volume numerical models used by energy companies

- ✓ Each fracture is subdivided into three regions: (1) “stick”: the fracture is closed and all components of traction are unknown; (2) “slip”: the fracture can slide but doesn’t open, only the normal component of traction is unknown; (3) “open”: the contact surfaces are inner traction-free boundaries
- ✓ The problem is highly non-linear because also the “stick”, “slip” and “open” portions of each fracture are unknown

Mathematical model

Discretization and solution algorithm

- ✓ An active-set strategy, identifying the stick, slip and open regions, is used to transform the variational inequality into a variational equality:

$$(\boldsymbol{\mu}, \boldsymbol{g})_{\Gamma_f^{stick}} + (\mu_N, g_N)_{\Gamma_f^{slip}} + \kappa(\boldsymbol{\mu}_T, \boldsymbol{t}_T - \tau_L \boldsymbol{g}_T / \|\boldsymbol{g}_T\|_2)_{\Gamma_f^{slip}} + \kappa(\boldsymbol{\mu}, \boldsymbol{t})_{\Gamma_f^{open}} = 0 \qquad \forall \boldsymbol{\mu} \in \boldsymbol{\mathcal{M}}(t_N)$$

- ✓ By introducing the discrete approximations $\boldsymbol{u}^h = \sum_i u_i \boldsymbol{\eta}_i$ and $\boldsymbol{t}^h = \sum_j t_j \boldsymbol{\mu}_j$, we obtain a non-linear system of discrete equations that is solved by using a Newton method

- ✓ On summary, we have three nested cycles to solve the proposed Boundary Value Problem:
  - Active-set iteration to identify the stick, slip, open regions
  - Newton iteration to solve the non-linear problem
  - Krylov iteration to solve the inner Jacobian system

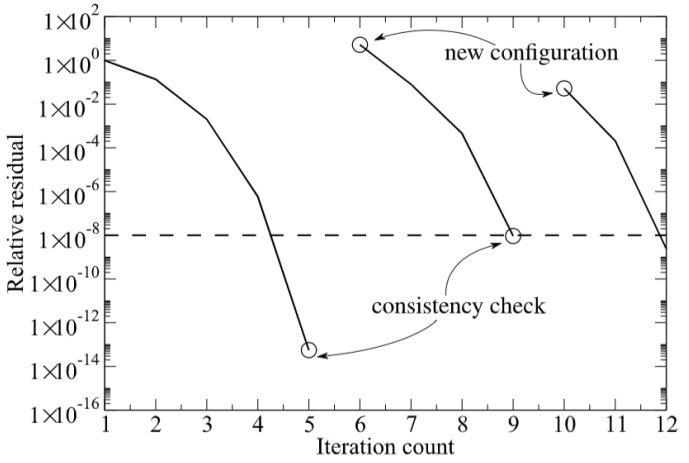

Mathematical model

Discretization and solution algorithm

- ✓ The low-order $\mathbb{Q}_1 - \mathbb{P}_0$ pair of spaces is not uniformly inf-sup stable, as it can be easily verified by a simple patch test (the kernel of the resulting Schur complement is not empty)
- ✓ As a consequence, the solution may suffer from the appearance of spurious traction modes with the classical «checkerboard» structure
- ✓ The problem can be addressed by introducing a local stabilization by extending the idea of the Jump Stabilization introduced for Stokes problems [Elman et al., 2014]

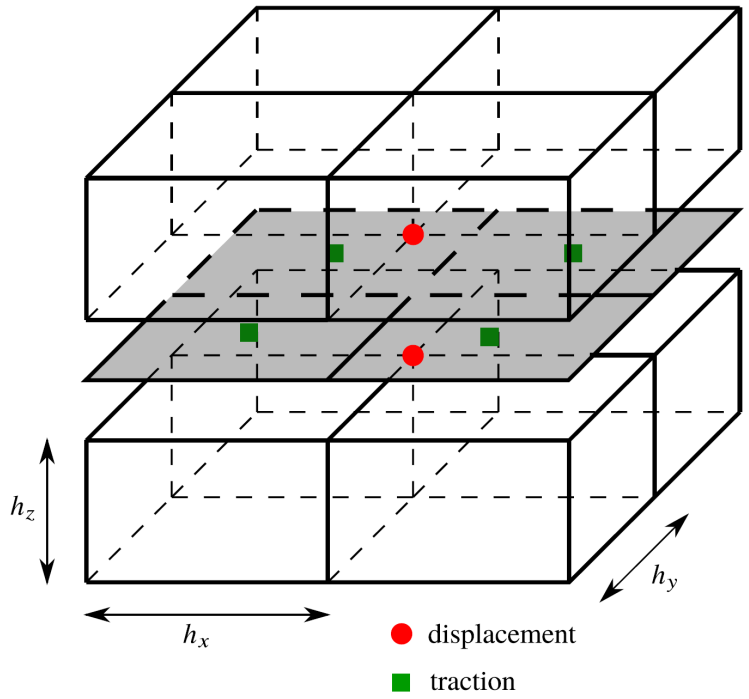

- ✓ We add a stabilization term to the discretized equation of equilibrium on the fault surface that, from a physical viewpoint, introduces a fictious force to balance the spurious traction modes and prescribing an element-wise equilibrated condition:

$$\left(\boldsymbol{\mu}_j, [\![\boldsymbol{u}^h]\!]\right)_{\Gamma_f^{stick}} + \left(\mu_{N,j}, [\![\boldsymbol{u}^h]\!] \cdot \boldsymbol{n}\right)_{\Gamma_f^{slip}} + \kappa\left(\boldsymbol{\mu}_{T,j}, \boldsymbol{t}_T^h - \boldsymbol{t}_T^*\right)_{\Gamma_f^{slip}} + \kappa\left(\boldsymbol{\mu}_j, \boldsymbol{t}^h\right)_{\Gamma_f^{open}} - \mathcal{J}\left(\boldsymbol{\mu}_j, \boldsymbol{t}^h\right) = 0 \qquad \forall \boldsymbol{\mu}_j \in \boldsymbol{\mathcal{M}}^h$$

Mathematical model

Discretization and solution algorithm

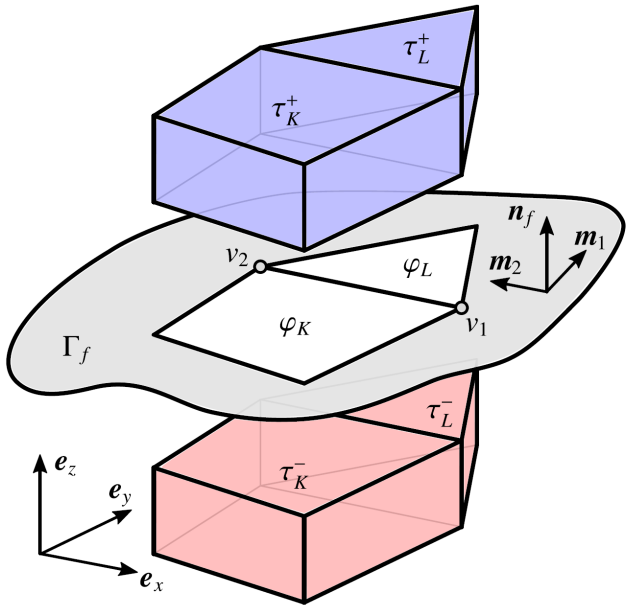

✓ The stabilization terms reads (Franceschini et al., 2022a):

$$\mathcal{J}(\boldsymbol{\mu}_j, \boldsymbol{t}^h) = \sum_e \frac{1}{|e|} \int_e [\![\boldsymbol{\mu}_j]\!]_e \cdot \boldsymbol{\Upsilon}^{(e)} \cdot [\![\boldsymbol{t}^h]\!]_e$$

for the edge e between two elements φ_K and φ_L, with $\boldsymbol{\Upsilon}^{(e)}$ a positive definite second-order tensor providing the appropriate scaling of the stabilization term as a function of the element size and material properties

✓ After linearization, the Jacobian system has a generalized saddle-point structure:

$$\begin{bmatrix} A & B_1 \\ B_2 & -H \end{bmatrix} \begin{bmatrix} \Delta \boldsymbol{u} \\ \Delta \boldsymbol{t} \end{bmatrix} = \begin{bmatrix} \boldsymbol{r_u} \\ \boldsymbol{r_t} \end{bmatrix}$$

- $A \in \mathbb{R}^{n_u \times n_u}$: tangent stiffness matrix (SPSD)
- $B_1 \in \mathbb{R}^{n_u \times n_t}$: force coupling block
- $B_2 \in \mathbb{R}^{n_t \times n_u}$: consistency coupling block
- $H \in \mathbb{R}^{n_t \times n_t}$: stabilization matrix (SPSD)

Mathematical model

Linear solver

- The standard and optimal way to address the preconditioning of a saddle-point matrix exploits its block LDU factorization and approximates the Schur complement [Murphy et al., 2000; Benzi et al., 2005]:

$$\mathcal{A}^{-1} = \begin{bmatrix} A & B_1 \\ B_2 & -H \end{bmatrix}^{-1} = \begin{bmatrix} I_u & -A^{-1}B_1 \\ 0 & I_t \end{bmatrix} \begin{bmatrix} A^{-1} & 0 \\ 0 & S^{-1} \end{bmatrix} \begin{bmatrix} I_u & 0 \\ -B_2A^{-1} & I_t \end{bmatrix}, \qquad S = H + B_2A^{-1}B_1$$

- The key for the preconditioner is to replace A^{-1} and S^{-1} with effective sparse approximations, but this is not easy for the problem at hand [Franceschini et al., 2019]:
  - a good sparse approximation of S, which is fully dense, often does not exist and, even if a sparse approximation of S is used, an off-the-shelf algebraic approximation for its inverse might not be available
  - in any case, this approach cannot be used if A is singular
- The idea is use as a preconditioner for $\mathcal{A}$ the symmetrized and stabilized matrix $\hat{\mathcal{A}}$ by a regular SPD matrix C:

$$\hat{\mathcal{A}} = \begin{bmatrix} A & B \\ B^T & -C \end{bmatrix}$$

Mathematical model

Linear solver

- ✓ Optimal selection of fictitious SPD stabilization matrix *C* [Franceschini et al., 2022b]:

> **Theorem.** *Let $\mathcal{A}$ and $\hat{\mathcal{A}}$ the saddle-point matrices defined above, with A non-singular. If $C = B^T A^{-1} B$, then the eigenvalues of the preconditioned matrix $\hat{\mathcal{A}}^{-1}\mathcal{A}$ are either 1, with multiplicity n_u, or 0.5, with multiplicity n_t*

- ✓ An idea for selecting C may rely on classical Augmented Lagrangian techniques, where $C = \gamma I_t$ and $\gamma = \|B\|_2^2 / \|A\|_2$
- ✓ A much-improved variant for C exploits a local definition of γ:

$$C_{i,i} = \frac{\|r(\boldsymbol{b}_i)\|_2^2}{\left\|A|_{\boldsymbol{b}_i}\right\|_2}$$

- ✓ The application of $\hat{\mathcal{A}}^{-1}$ is carried out by using its block UDL factorization, which gives rise to the so-called “primal” Schur complement $S_u \in \mathbb{R}^{n_u \times n_u}$ [Benzi et al., 2005]:

$$\hat{\mathcal{A}}^{-1} = \begin{bmatrix} A & B \\ B^T & -C \end{bmatrix}^{-1} = \begin{bmatrix} I_u & 0 \\ C^{-1}B^T & I_t \end{bmatrix} \begin{bmatrix} {S_u}^{-1} & 0 \\ 0 & -C^{-1} \end{bmatrix} \begin{bmatrix} I_u & BC^{-1} \\ 0 & I_t \end{bmatrix}, \qquad S_u = A + BC^{-1}B^T$$

Mathematical model

Linear solver

- ✓ The primal Schur complement S_u:
  - is SPD even if A is singular
  - preserves a workable sparsity
  - from a physical viewpoint, is a structural stiffness matrix with a modified stiffness around the fractures
- ✓ The inverse of S_u can be effectively applied in an approximate way by an off-the-shelf multigrid method
- ✓ The proposed algorithm uses a reverse approach with respect to classical constraint preconditioners, by exploiting the primal Schur complement of an augmented matrix (**Reverse Augmented Constraint Preconditioner – RACP**):

$$\mathcal{M}^{-1} = \begin{bmatrix} I_u & 0 \\ C^{-1}B^T & I_t \end{bmatrix} \begin{bmatrix} \tilde{S}_u^{-1} & 0 \\ 0 & -C^{-1} \end{bmatrix} \begin{bmatrix} I_u & BC^{-1} \\ 0 & I_t \end{bmatrix}$$

- ✓ The cost of the RACP application is practically equal to the application of $\tilde{S}_u^{-1}$ to a vector, e.g. the complexity of a multigrid operator

Mathematical model

Linear solver

Theorem. *Let $\mathcal{A}$ and $\mathcal{M}^{-1}$ the saddle-point matrix and RACP defined above, and:*

$$\alpha_u = \lambda_{\min}\left(\tilde{S}_u^{-1}(S_u + BC^{-1}B^T)\right), \qquad \beta_u = \lambda_{\max}\left(\tilde{S}_u^{-1}(S_u + BC^{-1}B^T)\right),$$
$$\alpha_t = \sigma_{\min}\left(\tilde{S}_u^{-1/2}BC^{-1/2}\right), \qquad \beta_t = \sigma_{\max}\left(\tilde{S}_u^{-1/2}BC^{-1/2}\right),$$

where λ and σ denote the eigenvalues and the singular values, respectively. The, the real eigenvalues of $\mathcal{M}^{-1}\mathcal{A}$ are such that:

$$\min\left\{\alpha_u, \frac{2\alpha_t^2}{\beta_u + \sqrt{\beta_u^2 - 4\alpha_t^2}}\right\} \leq \lambda \leq \beta_u,$$

and the real and imaginary parts of the complex eigenvalues are such that:

$$\frac{\alpha_u}{2} \leq Re(\lambda) \leq \frac{\beta_u}{2}, \qquad |Im(\lambda)| \leq \sqrt{\beta_t^2 - \frac{\alpha_u^2}{4}},$$

with no complex eigenvalues if $2\beta_t < \alpha_u$.

Proof. See Franceschini et al., 2022b.

Mathematical model

Linear solver

✓ Eigenspectrum of $\mathcal{M}^{-1}\mathcal{A}$ with $\tilde{S}_u^{-1} = S_u^{-1}$ (left) and $\tilde{S}_u^{-1} = \mathrm{AMG}(S_u)$ (right) as compared to the theoretical bounds:

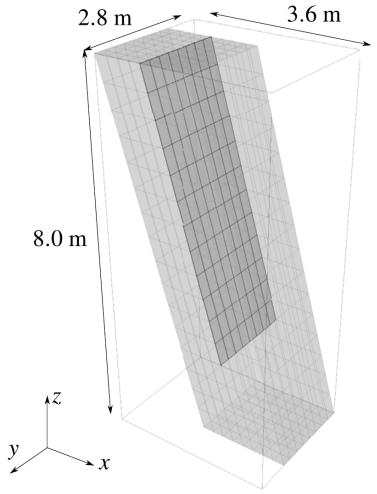

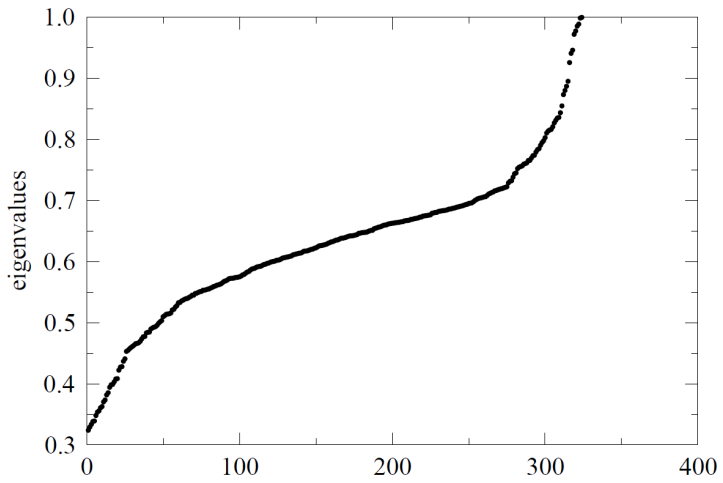

effect of the choice for C

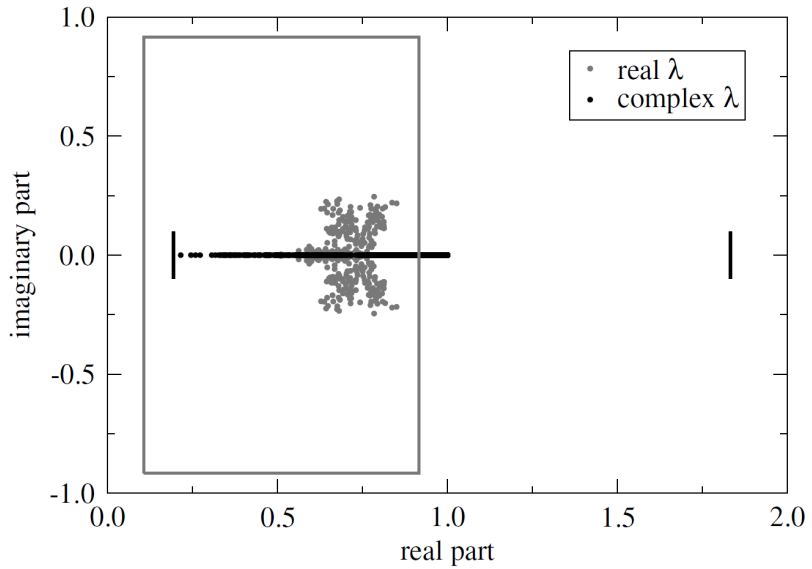

effect of the use of AMG

Numerical results

Solver performance

✓ Effect of the augmentation on the conditioning of A and S_u:

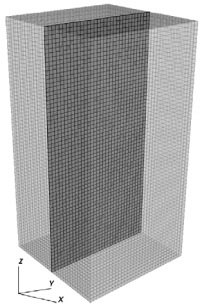

A

$n_u = 218{,}790$
$n_t = 6{,}336$
(2.9%)

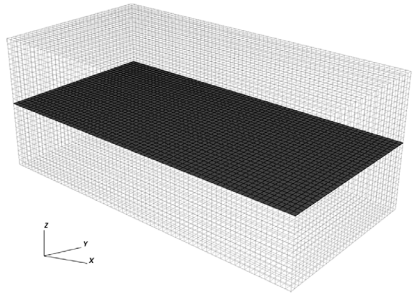

B

$n_u = 194{,}208$
$n_t = 6{,}936$
(3.6%)

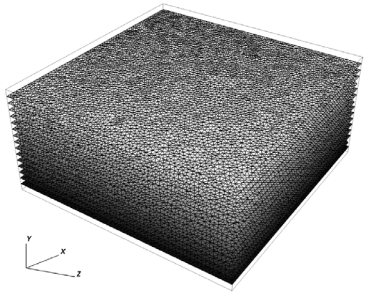

C

$n_u = 379{,}983$
$n_t = 167{,}799$
(44.2%)

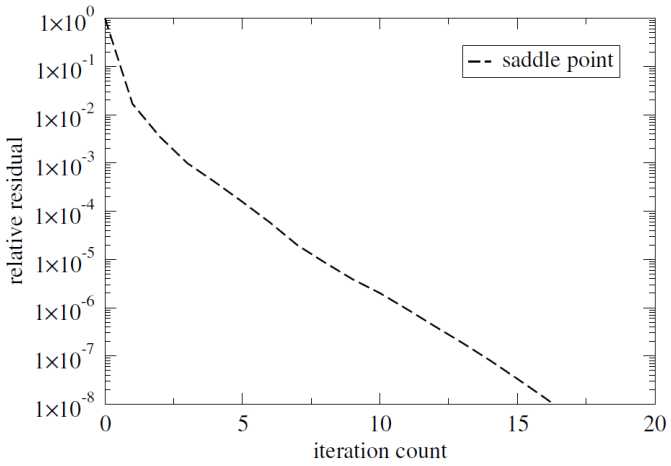

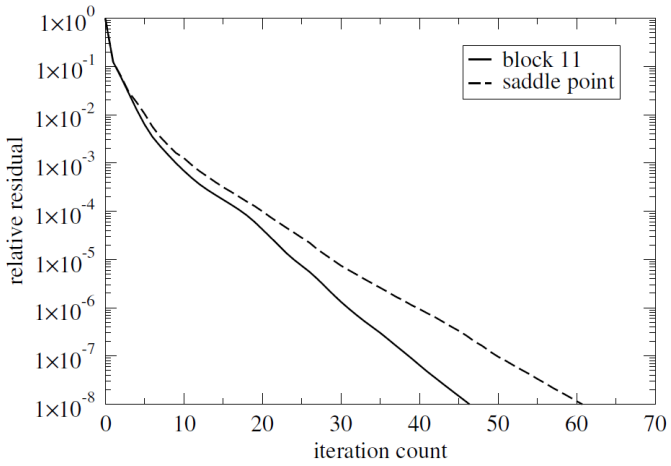

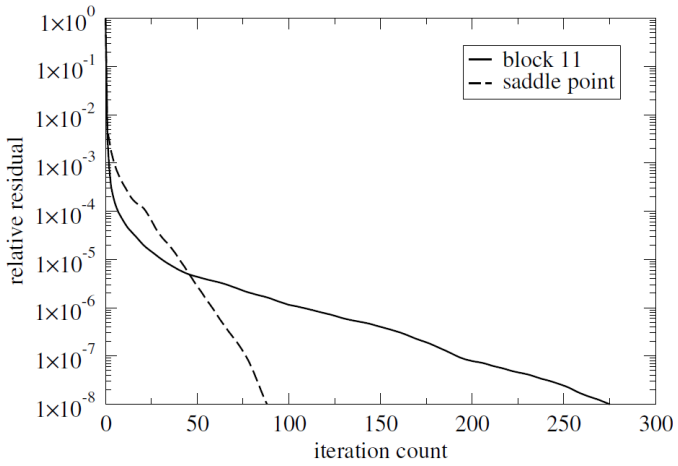

Numerical results

Solver performance

- ✓ Comparison of the RACP computational efficiency with the outcome obtained by the «standard» approach (Mixed Constraint Preconditioner – MCP) [Franceschini et al, 2019]
- ✓ To approximate the application of A^{-1} and S^{-1} either AMG or FSAI is used (MCP+AMG and MCP+FSAI)
- ✓ The preconditioner application cost c_{app} denotes the number of matrix-vector products with the matrix $\mathcal{A}$ required to compute $\mathcal{M}^{-1}\,\boldsymbol{r}$, while the total cost C_s is computed as C_s=n_{it} (1+c_{app})

	RACP			MCP+AMG			MCP+FSAI		
Test	n_{it}	c_{app}	C_s	n_{it}	c_{app}	C_s	n_{it}	c_{app}	C_s
A	17	5.36	108.12	X	-	-	X	-	-
B	61	4.21	317.81	153	8.43	1442.79	> 1,000	1.85	X
C	89	4.52	491.28	> 1,000	9.51	X	270	3.18	1128.60

Numerical results

Solver performance

- ✓ Mesh independence analysis when progressively refining the discretization size

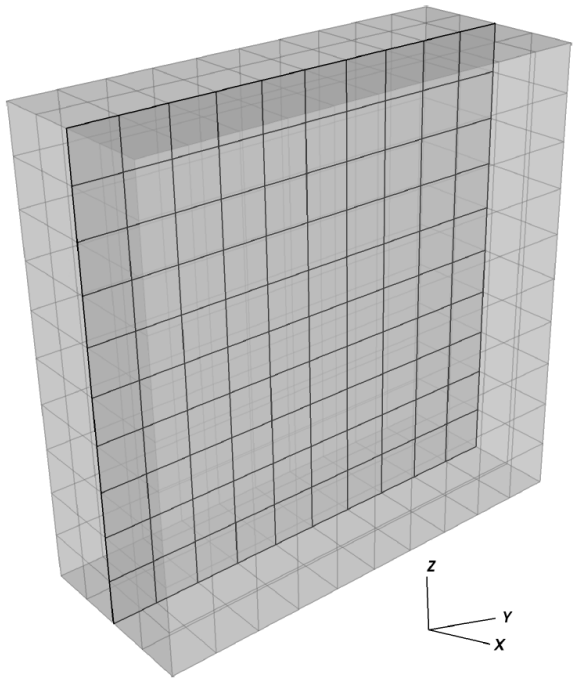

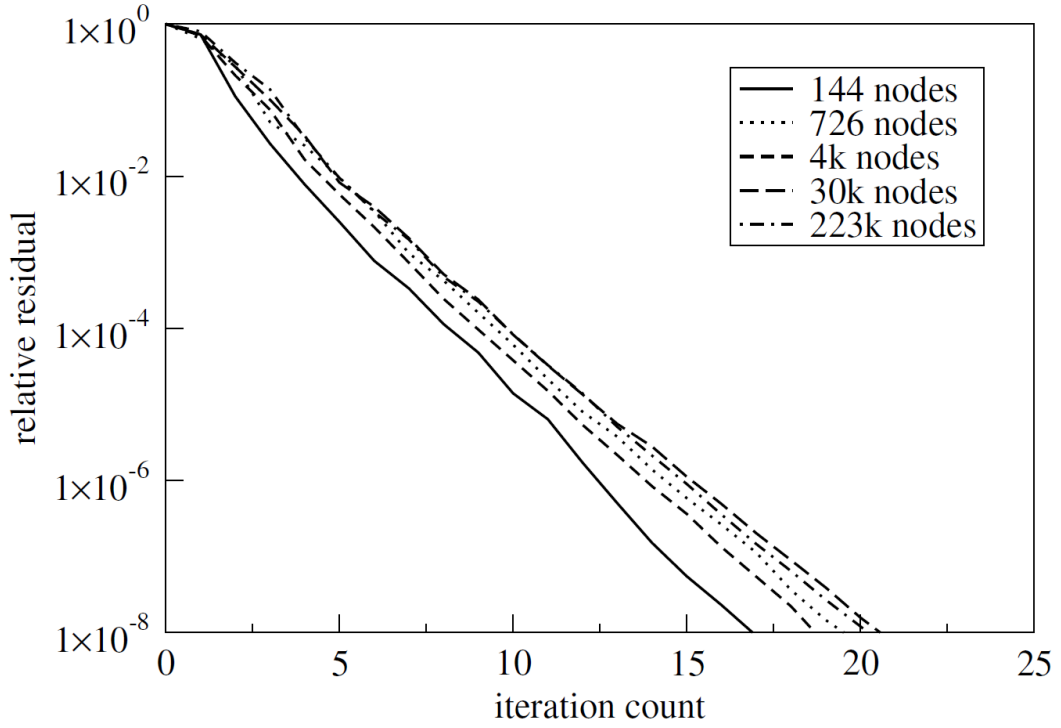

Numerical results

Solver performance

- ✓ An efficient parallel implementation of RACP is fundamental for solving large size problems that could arise in several applications
- ✓ Most of the operations that need to be parallelized in RACP can be borrowed from existing libraries, the only one that requires an ad hoc implementation is the computation of the diagonal entries of C
- ✓ The parallel implementation relies on the Chronos library [Isotton et al., 2021], whose use for research purposes is free of charge (www.m3eweb.it/chronos)
- ✓ Partition of A, B and B^T is carried out with the aid of the ParMETIS library, so as to minimize communications
- ✓ Lagrange multipliers are assigned to each process so as to collect as many entries as possible for the computation of the C elements locally

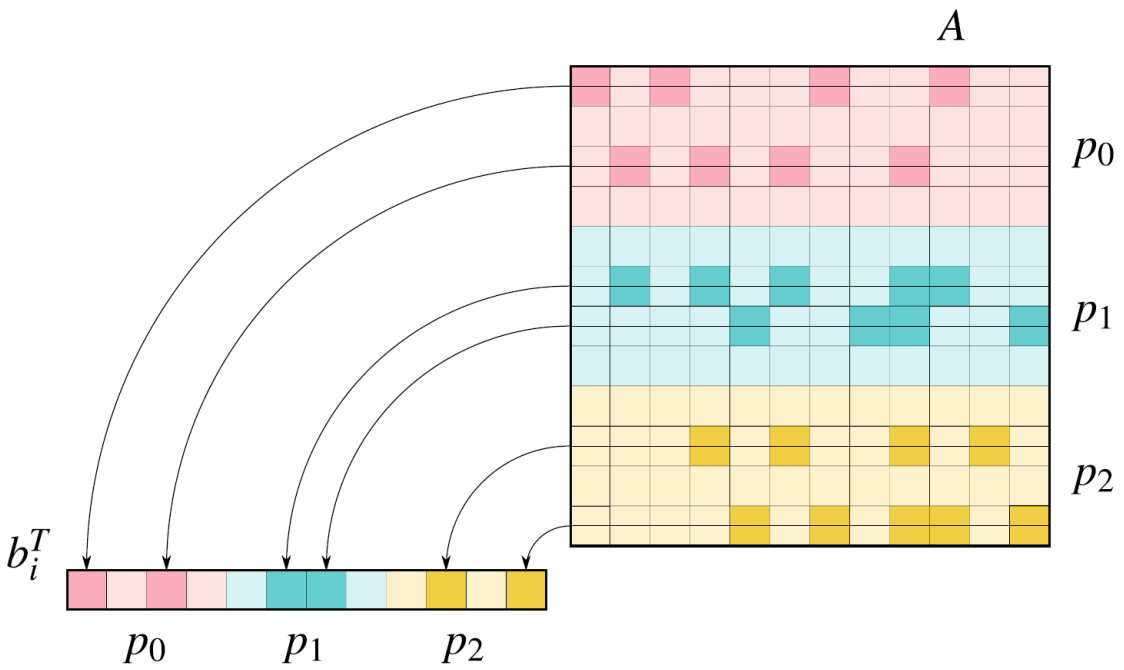

Numerical results

Solver performance

- ✓ Weak and strong scalability tests with RACP and Chronos AMG

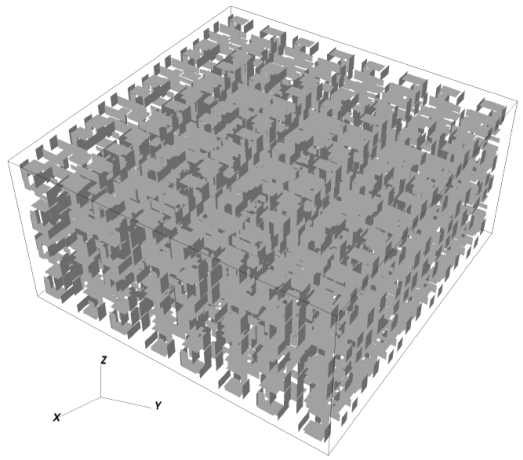

$n_u = 73{,}042{,}971$
$n_t = 10{,}553{,}856$
(14.4%)

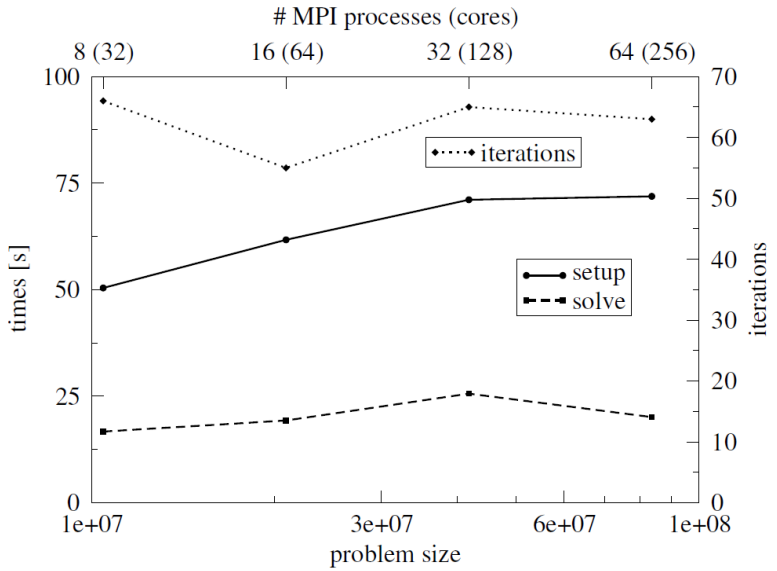

Weak scalability

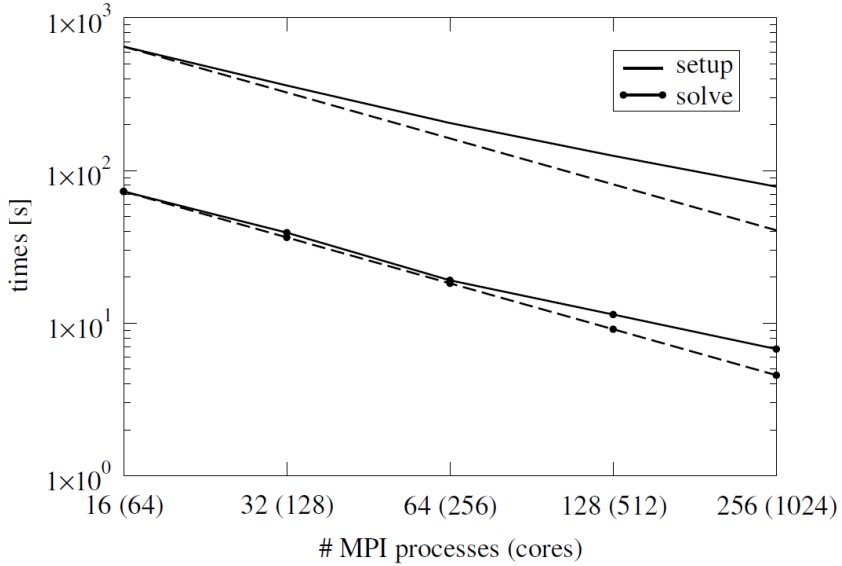

Strong scalability

Mathematical model

Governing PDEs, variational formulation and discretization

- ✓ The model is updated by introducing the fluid flow in the fractures:

$$-\nabla \cdot \boldsymbol{\sigma}(\boldsymbol{u}) = \boldsymbol{b} \qquad \forall\, (\boldsymbol{x}, t) \in \Omega \times [0, T] \qquad \text{(linear momentum balance)}$$

$$g_N(\boldsymbol{u}) + \nabla \cdot \boldsymbol{q}(\boldsymbol{u}, p) = q_s \qquad \forall\, (\boldsymbol{x}, t) \in \Gamma_f \times [0, T] \qquad \text{(mass balance on the fracture)}$$

$$\boldsymbol{\sigma}(\boldsymbol{u}) \cdot \boldsymbol{n}_f = p\boldsymbol{n}_f \qquad \forall\, (\boldsymbol{x}, t) \in \Gamma_f \times [0, T] \qquad \text{(traction balance on the fracture)}$$

being the fractures subject to the same impenetrability and friction conditions set previously

- ✓ The fluid flow in the fractures is modelled by the classical Darcy relationship $\boldsymbol{q}(\boldsymbol{u}, p) = -\left[C_f(\boldsymbol{u})/\mu\right]\nabla p$, where the fracture conductivity is related to the displacement by a cubic law [Garipov et al., 2016]:

$$C_f(\boldsymbol{u}) = C_{f,0} + \frac{(\llbracket \boldsymbol{u} \rrbracket \cdot \boldsymbol{n})^3}{12}$$

- ✓ Mass balance equation is discretized by a Finite Volume scheme (TPFA) in order to locate pressure variables where tractions are defined

Mathematical model

Governing PDEs, variational formulation and discretization

- Weak variational formulation:

$$(\boldsymbol{\nabla}^s\boldsymbol{\eta},\boldsymbol{\sigma})_\Omega + \sum_{i=1}^{n_f}\left([\![\boldsymbol{\eta}]\!],\boldsymbol{t}^h - p^h\boldsymbol{n}_i\right)_{\Gamma_f} = (\eta,b)_\Omega + (\boldsymbol{\eta},\bar{\boldsymbol{t}})_{\Gamma_\sigma} = 0 \qquad \forall\,\boldsymbol{\eta}\in\boldsymbol{\mathcal{U}}_0\subset[H^1(\Omega)]^3$$

$$(t_N^h - \mu_N, g_N)_{\Gamma_f} + \left(\boldsymbol{t}_T^h - \boldsymbol{\mu}_T, \Delta\boldsymbol{g}_T\right)_{\Gamma_f} \geq 0 \qquad \forall\,\boldsymbol{\mu}\in\boldsymbol{\mathcal{M}}(t_N)$$

$$\left(\chi,\frac{\Delta g_N}{\Delta t}\right)_{\Gamma_f} + [\chi,p^h]_{\mathcal{F}} - F_{\mathcal{F}}(\chi) + G_{\mathcal{F}}(\chi) - (\chi,q_s)_{\Gamma_f} = 0 \qquad \forall\,\chi\in\mathcal{P}_0\subset L^2(\Omega)$$

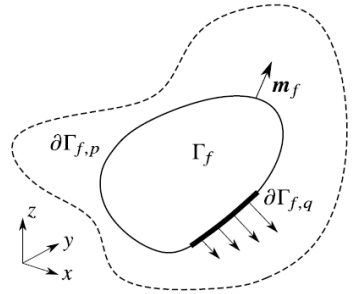

- The last equation introduces a weighted inner product formally reproducing the TPFA operator in a variational fashion:

$$[\chi,p^h]_{\mathcal{F}} = \sum_e \left(\chi\big|_K - \chi\big|_L\right)\mathrm{K}^{KL}\left(p^h\big|_K - p^h\big|_L\right)$$

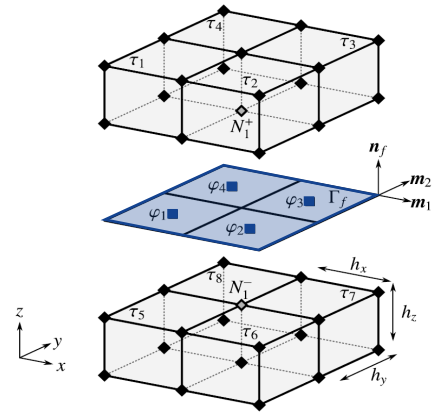

Mathematical model

Governing PDEs, variational formulation and discretization

- ✓ As for the tractions, also spurious modes in the pressure solution may arise in undrained and incompressible conditions with the low-order inf-sup unstable selected pair
- ✓ We introduce the same stabilization as for the tractions, now balancing the jumps in the elemental pressure values [Franceschini et al., 2020]:

$$\mathcal{J}(\chi_j, p^h) = \sum_e \frac{1}{|e|} \int_e \left[\!\left[\chi_j\right]\!\right]_e \cdot \Upsilon^{(e)} \cdot \left[\!\left[p^h\right]\!\right]_e$$

which is added to the discrete form of the mass balance equation

- ✓ The proposed formulation has the advantage of avoiding any interpolation between traction and pressure fields
- ✓ Again, we set up a nested three-cycle procedure: (i) active-set iteration to identify the status of the fracture, (ii) Newton iteration to solve the resulting set of non-linear equations, (iii) Krylov iteration to solve the inner linear system with the Jacobian matrix

Mathematical model

Governing PDEs, variational formulation and discretization

- ✓ At a given active-set iteration l, we set the Newton iteration:

$$\text{Solve} \quad \begin{bmatrix} A & B_1 & Q_1 \\ B_2 & -H & 0 \\ Q_2 & 0 & T \end{bmatrix}^{l,(k)} \begin{bmatrix} \delta \boldsymbol{u} \\ \delta \boldsymbol{t} \\ \delta \boldsymbol{p} \end{bmatrix} = - \begin{bmatrix} \boldsymbol{r}_u \\ \boldsymbol{r}_t \\ \boldsymbol{r}_p \end{bmatrix}^{l,(k)} \quad \text{and update} \quad \begin{bmatrix} \boldsymbol{u} \\ \boldsymbol{t} \\ \boldsymbol{p} \end{bmatrix}^{l,(k+1)} = \begin{bmatrix} \boldsymbol{u} \\ \boldsymbol{t} \\ \boldsymbol{p} \end{bmatrix}^{l,(k)} + \begin{bmatrix} \delta \boldsymbol{u} \\ \delta \boldsymbol{t} \\ \delta \boldsymbol{p} \end{bmatrix}$$

- ✓ 3x3 Jacobian block structure:

$$\begin{bmatrix} A & B_1 & Q_1 \\ B_2 & -H & 0 \\ Q_2 & 0 & T \end{bmatrix}$$

A : the elastic stiffness matrix (SPSD)

B_1 : the surface measure of the interface elements

Q_1 : the projection of B_1 along the normal direction to the fracture

B_2 : $B_1{}^T$ plus the frictional law derivatives in slip areas

H : the stabilization for the displacement-traction fields (SPSD)

Q_2 : the accumulation term derivative in open areas

T : the 5-point stencil transmissibility matrix plus the stabilization (SPD)

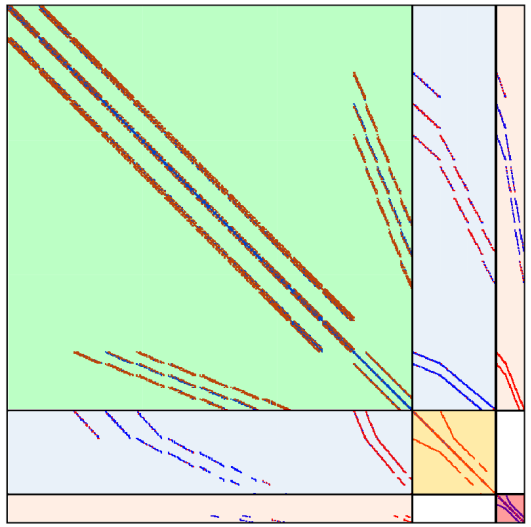

Mathematical model

Linear solver

- The preconditioner is the approximate block LDU factorization of the Jacobian matrix:

$$\begin{bmatrix} -H & B_2 & 0 \\ B_1 & A & Q_1 \\ 0 & Q_2 & T \end{bmatrix} \cong \begin{bmatrix} I_t & 0 & 0 \\ -BC^{-1} & I_u & 0 \\ 0 & Q_2 S_u^{-1} & I_p \end{bmatrix} \begin{bmatrix} -C & 0 & 0 \\ 0 & S_u & 0 \\ 0 & 0 & S_p \end{bmatrix} \begin{bmatrix} I_t & -C^{-1}B^T & 0 \\ 0 & I_u & S_u^{-1}Q_1 \\ 0 & 0 & I_p \end{bmatrix}$$

$$S_u = A + BC^{-1}B^T$$

$$S_p = T - Q_2 {S_u}^{-1} Q_1$$

- Matrix H is replaced with the diagonal local Augmented Lagrangian matrix C as before, while $Q_2 S_u^{-1} Q_1$ is approximated by an algebraic “fixed-stress” approach
- S_u is symmetric positive definite by construction, while S_p can be indefinite with open fractures ($Q_2 \neq 0$)
- In the preconditioner application, the inverse of S_u is applied by an AMG approach and the inverse of S_p by a nested direct solver because of its 2D connection topology and small size

Mathematical model

Linear solver

- ✓ The “fixed-stress” approach arises from coupled linear poroelasticity (discrete Biot’s model):

$$K\boldsymbol{u} - Q\boldsymbol{p} = \boldsymbol{f}$$
$$H\boldsymbol{p} + P\dot{\boldsymbol{p}} + Q^T\dot{\boldsymbol{u}} = \boldsymbol{q}$$
$$\Rightarrow \quad H\boldsymbol{p} + (P + Q^T K^{-1} Q)\dot{\boldsymbol{p}} = \boldsymbol{q} - Q^T K^{-1}\dot{\boldsymbol{f}}$$

- ✓ If there is no variation in time of the volumetric stress (“fixed-stress”), then $K_b \nabla \cdot \dot{\boldsymbol{u}} = b\dot{p}$, hence replacing in the discrete mass balance equation yields:

$$H\boldsymbol{p} + (P + M)\dot{\boldsymbol{p}} = \boldsymbol{q}$$

where *M* is a mass matrix depending on the material parameter b^2/K_b

- ✓ The idea is to replace the contribution $Q^T K^{-1} Q$ with the mass matrix *M* for the sake of preconditioning
- ✓ The “fixed-stress” approach can be generalized whenever we replace the discrete product $div^h \cdot \nabla_h^{-2} \cdot grad^h$ with a mass matrix with a proper scaling

Mathematical model

Linear solver

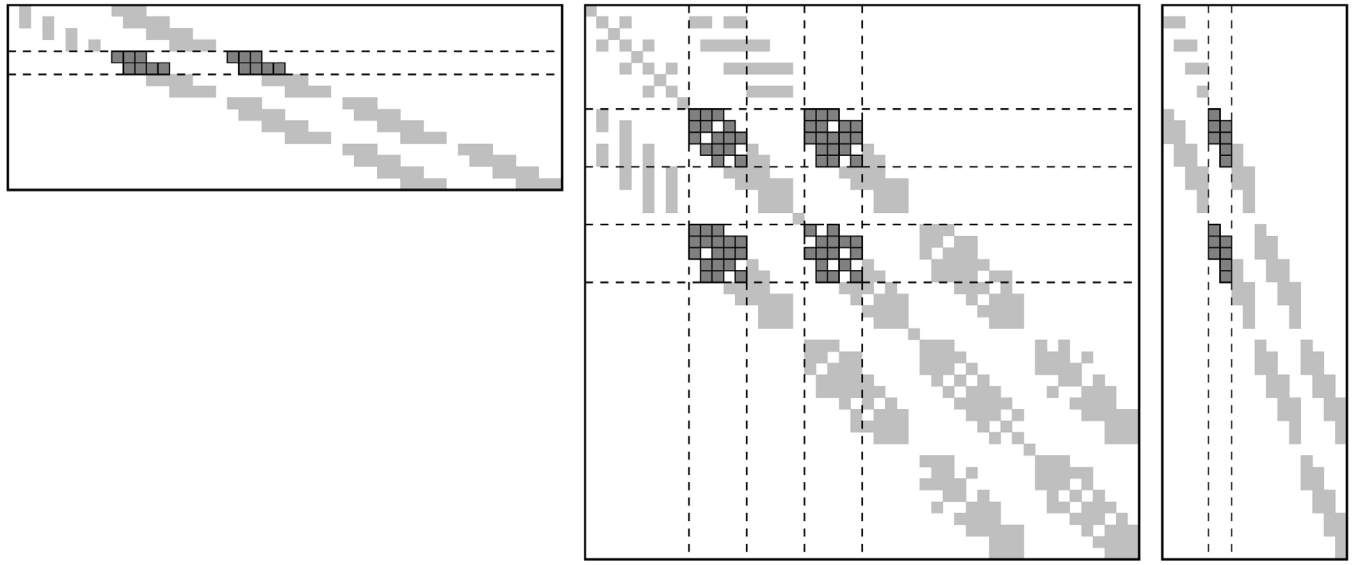

- ✓ For a general problem, it can be non-trivial to identify the most appropriate scaling of *M*
- ✓ We can use a fully algebraic interpretation of the mass matrix used in the «fixed-stress» approach, which allows for an automatic computation of the required scaling [Castelletto et al., 2016]

✓ Consider a set of m adjacent rows $Q_2^{(i)}$ and adjacent columns $Q_1^{(i)}$, the i-th $m \times m$ diagonal block of *M* reads:

$$M^{(i)} = r\left(Q_2^{(i)}\right) S_1|_i^{-1} r\left(Q_1^{(i)}\right)$$

or, if $S_1|_i$ is rectangular or rank-deficient

$$m^{(i)} = \left\| Q_1^{(i)} \right\| \left\| Q_2^{(i)} \right\| / \| S_1|_i \|$$

where *r* is the restriction operator keeping only the non-zeros of either a vector or a matrix *X*, and $S_1|_i$ is the restriction of S_1 to the rows and columns corresponding to the positions of the non-zero entries of *X*

Numerical results

Solver performance

- ✓ Weak scalability is investigated considering one refinement level for a structured mesh with 4 fractures

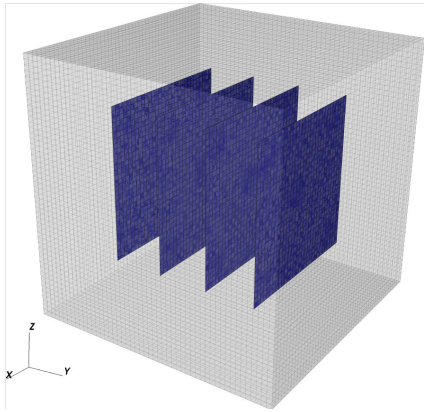

case	coarse	fine
n_u	55080	408045
n_t	2700	10800
n_p	900	3600
n_n	58680	422445

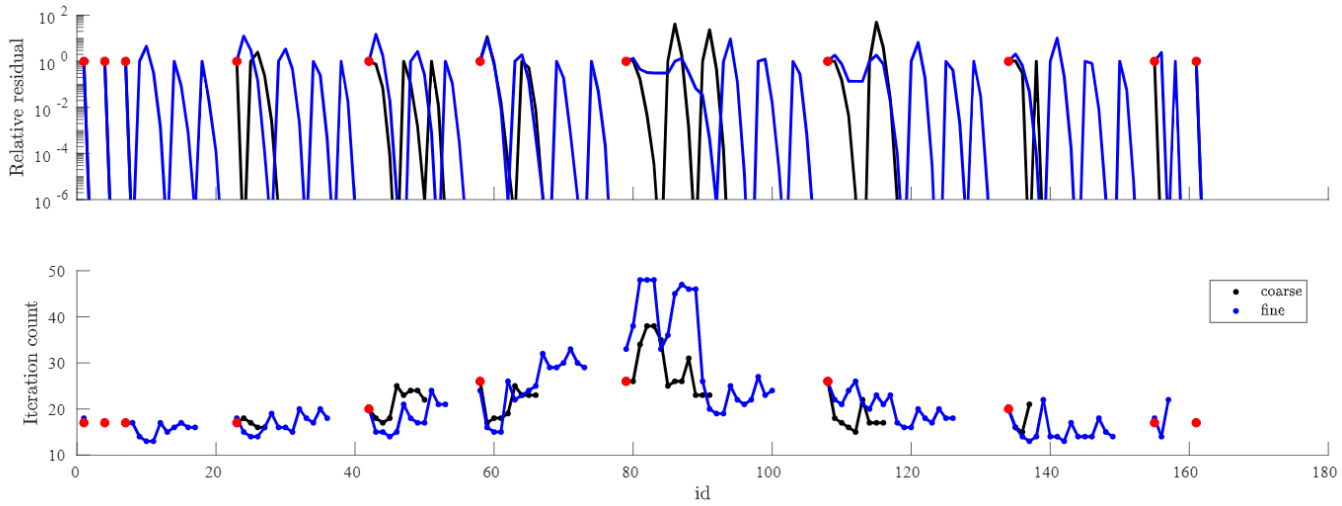

Comparison of non-linear convergence profiles and linear iterations

Numerical results

Solver performance

✓ The algorithm is tested for different ratios between fracture and 3D mesh sizes

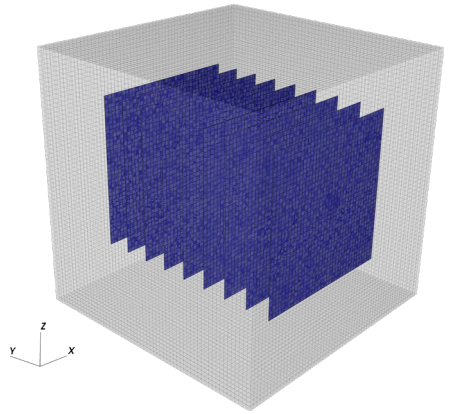

Number of linear iterations for each refinement level

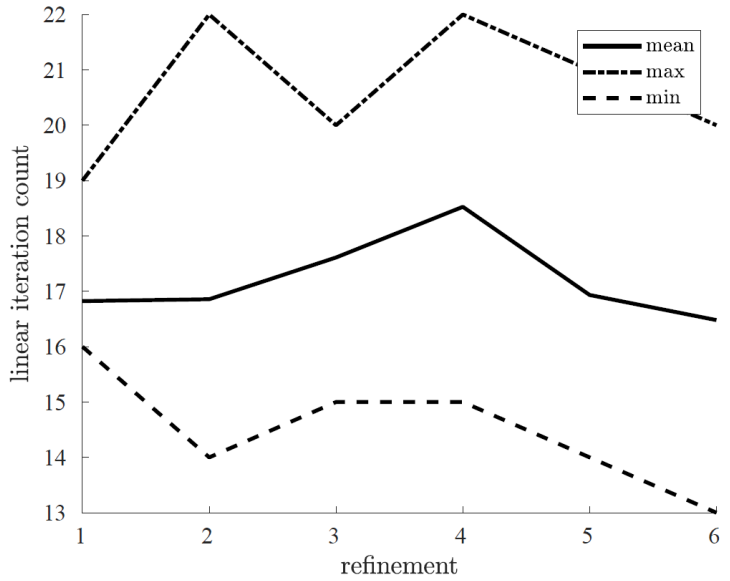

n_u	4668	31050	97176	221046	420600	714018
n_t	972	3888	8749	15552	24300	34992
n_p	324	1296	2916	5184	8100	11664
n_n	5964	36234	108840	241782	453060	760674
3D	78.3%	85.7%	89.3%	91.4%	92.8%	93.9%
2D	21.7%	14.3%	10.7%	8.6%	7.2%	6.1%

Numerical results

Solver performance

- ✓ A tilted well intersecting several fractures is tested, with a linearly increasing flow rate injected for the first 3 s before being withdrawn

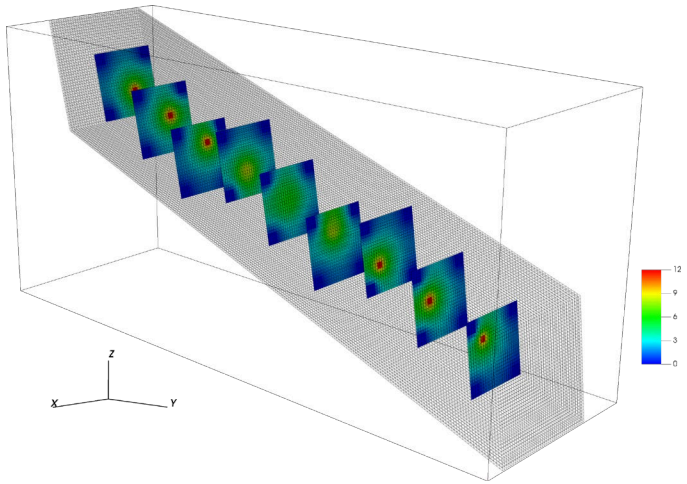

n_u	1,027,926
n_t	15,552
n_p	5,184
n_n	1,048,662

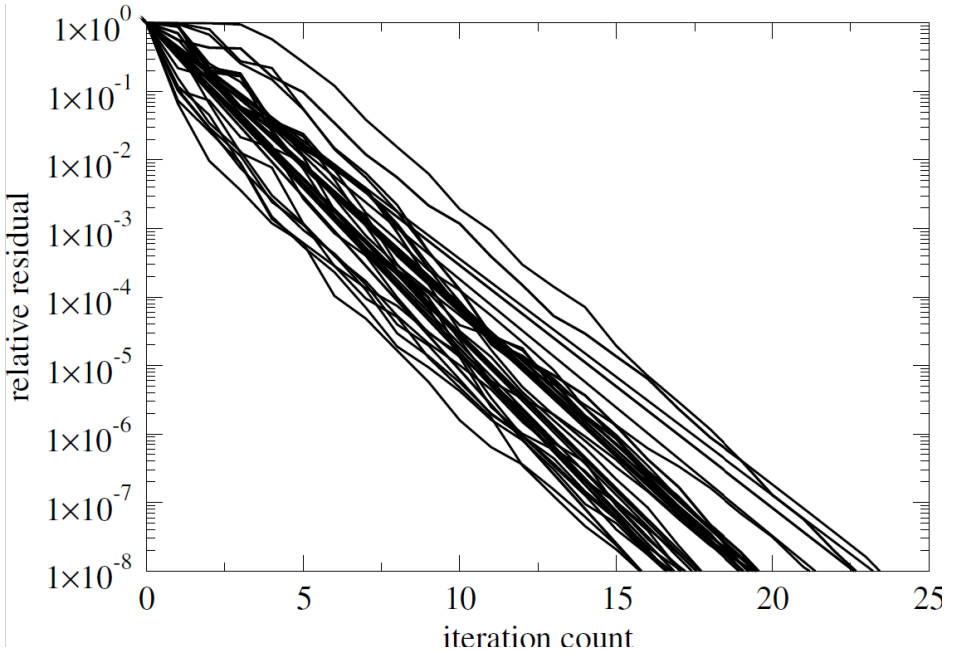

Numerical results

Validation, stability and convergence

✓ Validation against analytical solutions for frictional behavior

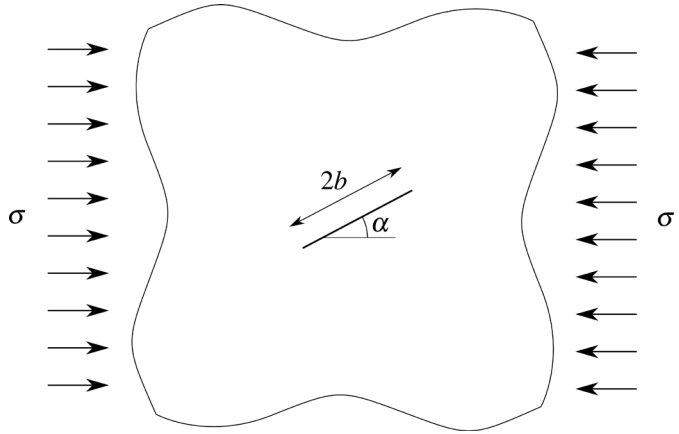

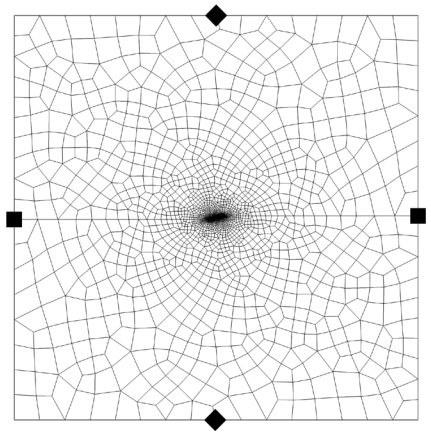

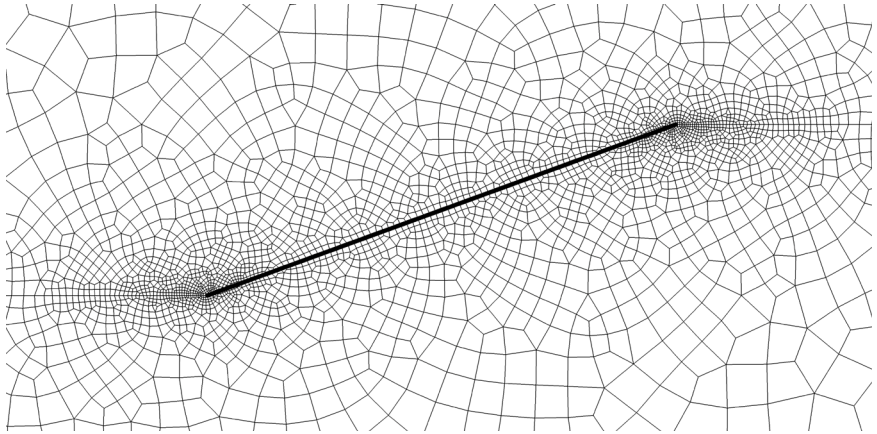

Sliding

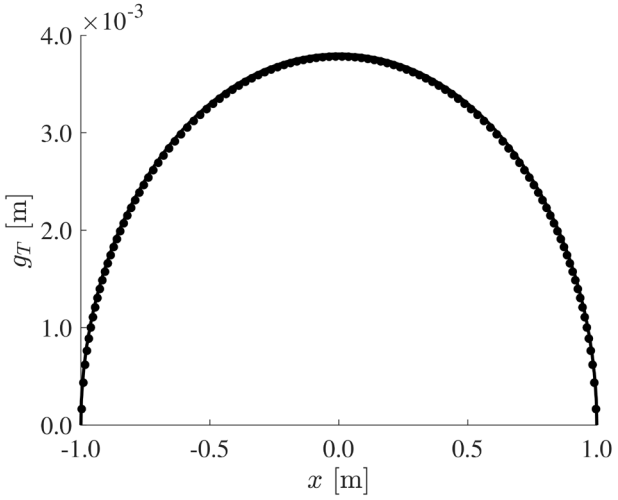

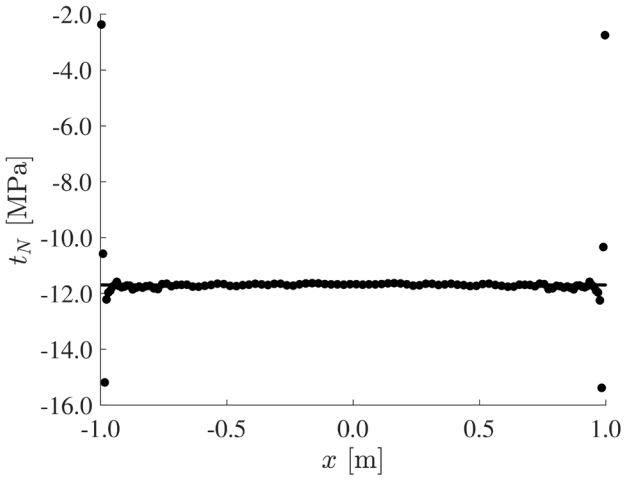

Normal traction

Numerical results

Validation, stability and convergence

✓ Validation against analytical solutions for normal behavior

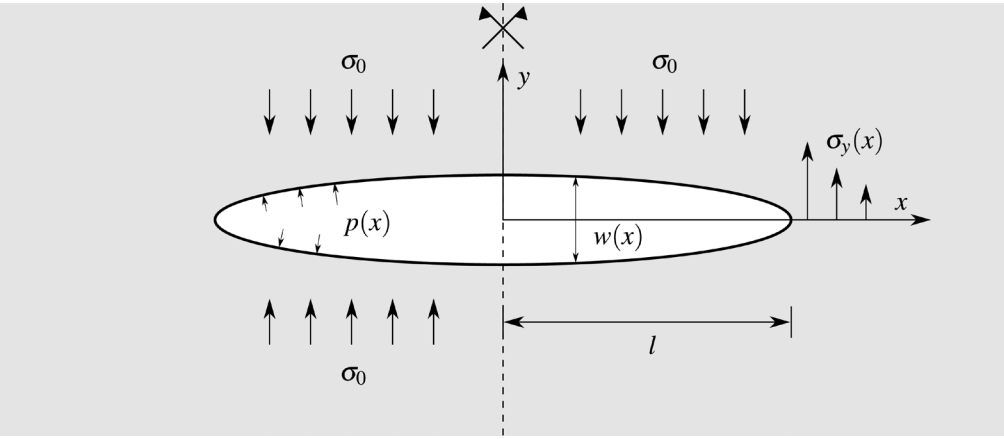

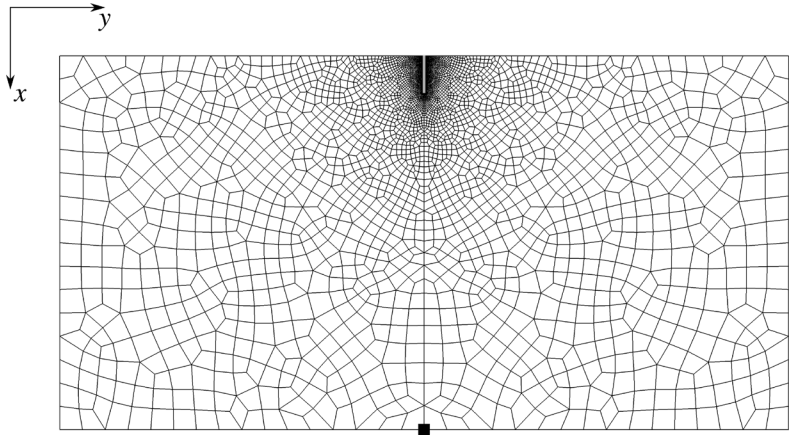

Opening

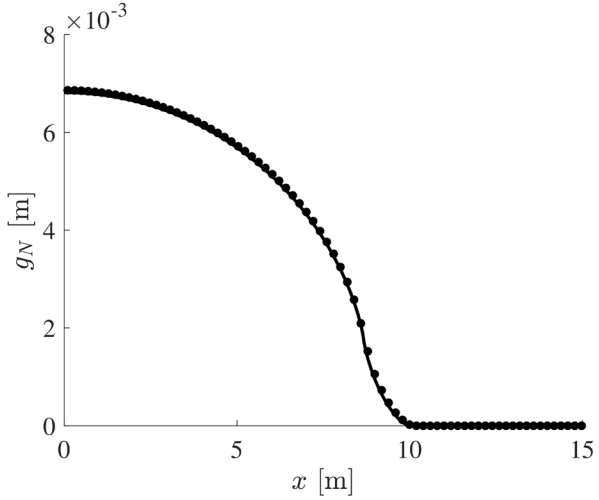

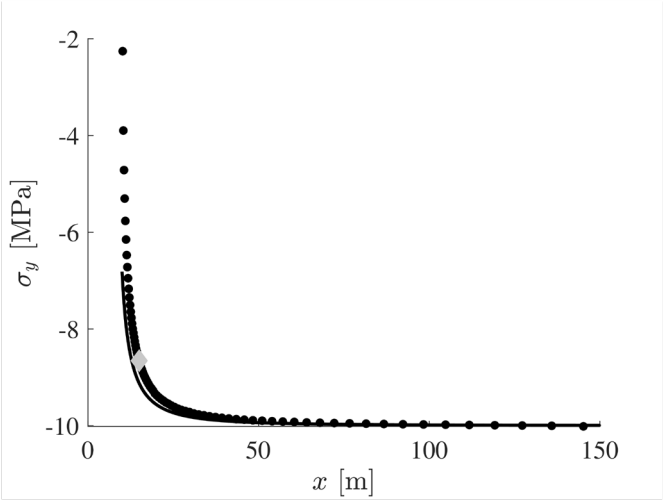

Normal traction

Numerical results

Validation, stability and convergence

- ✓ Convergence rate for sliding, traction and energy norm

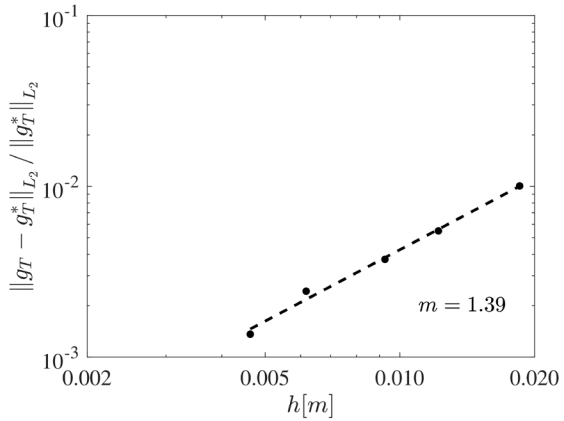

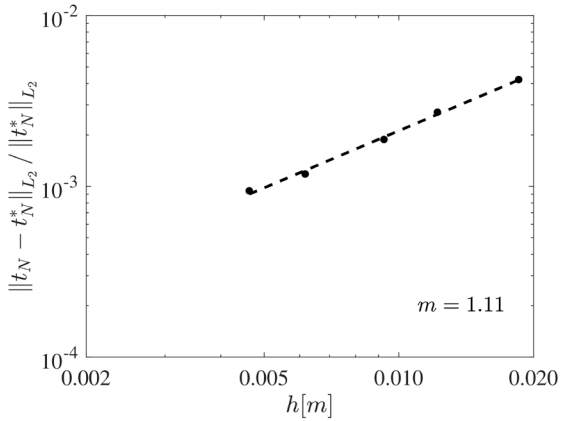

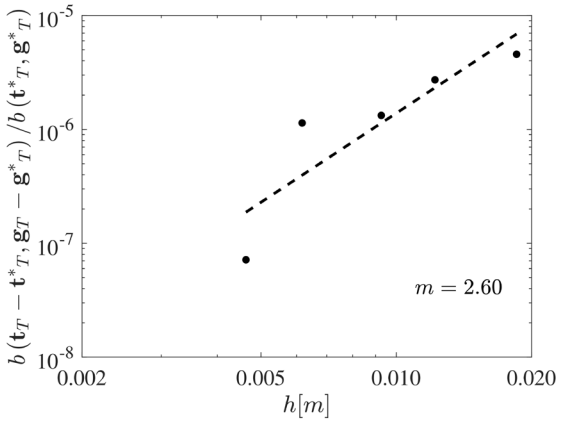

Frictional behavior

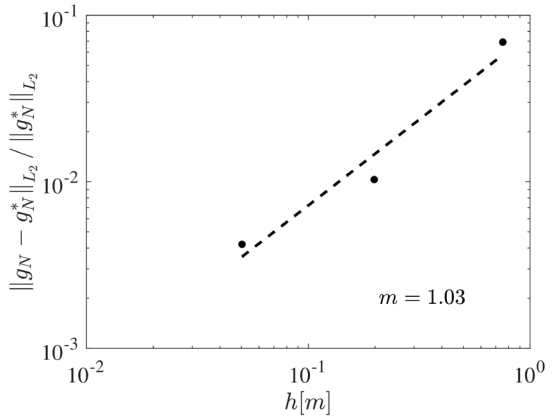

Normal behavior

Numerical results

Applications: ground ruptures due to groundwater pumping

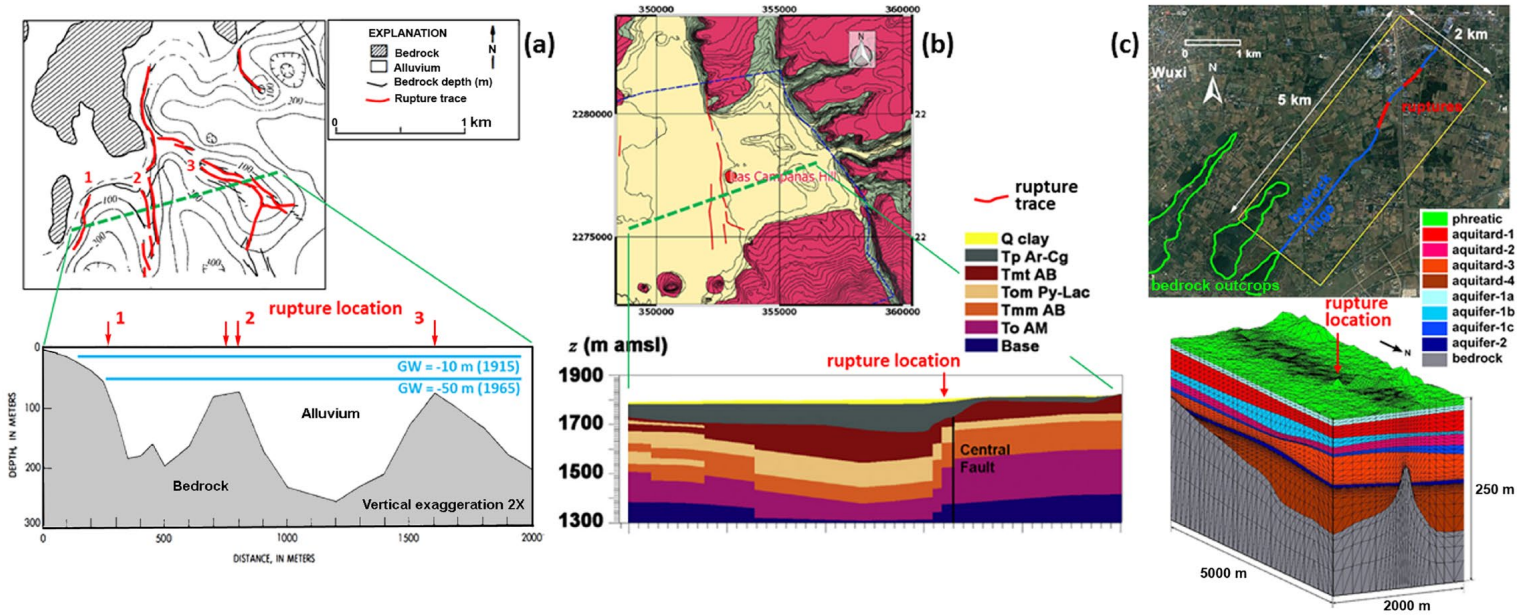

- ✓ Simulation of ground ruptures due to groundwater pumping:
  - Casa Grande, Arizona
  - Queretaro, Mexico
  - Wuxi, China

- ✓ Ruptures caused by emerging bedrocks, abrupt thickness changes and buried ridges

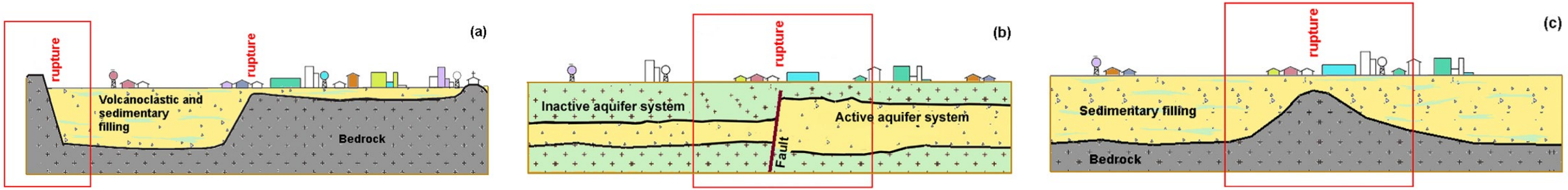

Numerical results

Applications: ground ruptures due to groundwater pumping

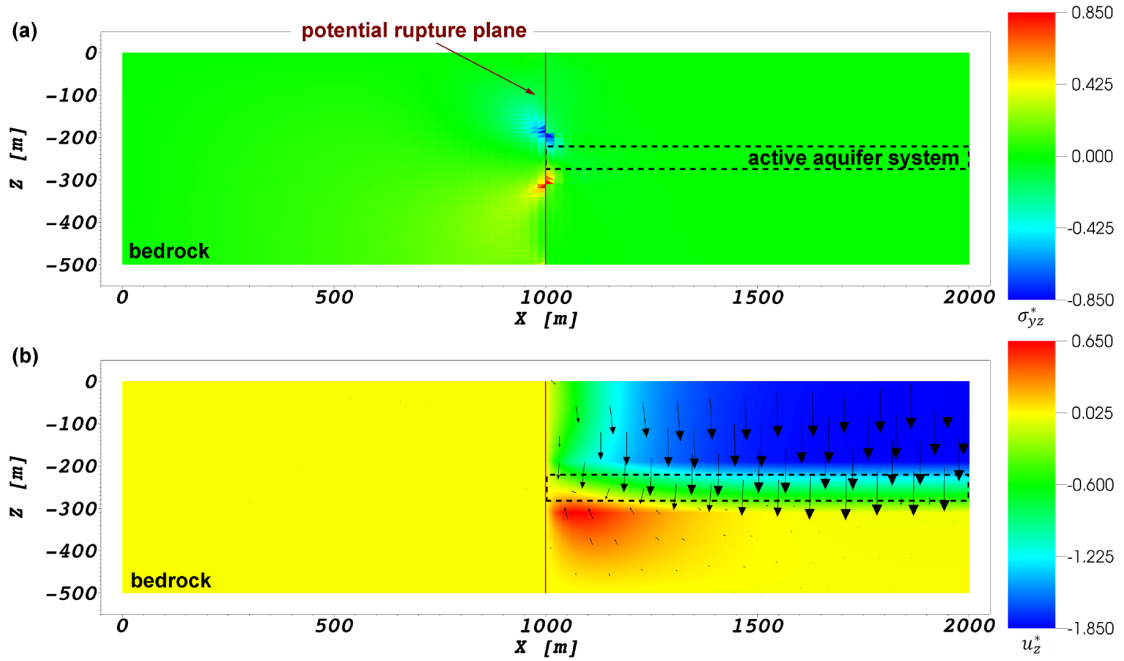

- ✓ Ruptures are more likely for thick and shallow aquifers
- ✓ One initiated, rupture propagation is essentially governed by the pressure decline in the aquifer

- ✓ Shear stress and vertical displacements with emerging bedrocks and abrupt changes in the aquifer thickness, which cause the generation of ground ruptures

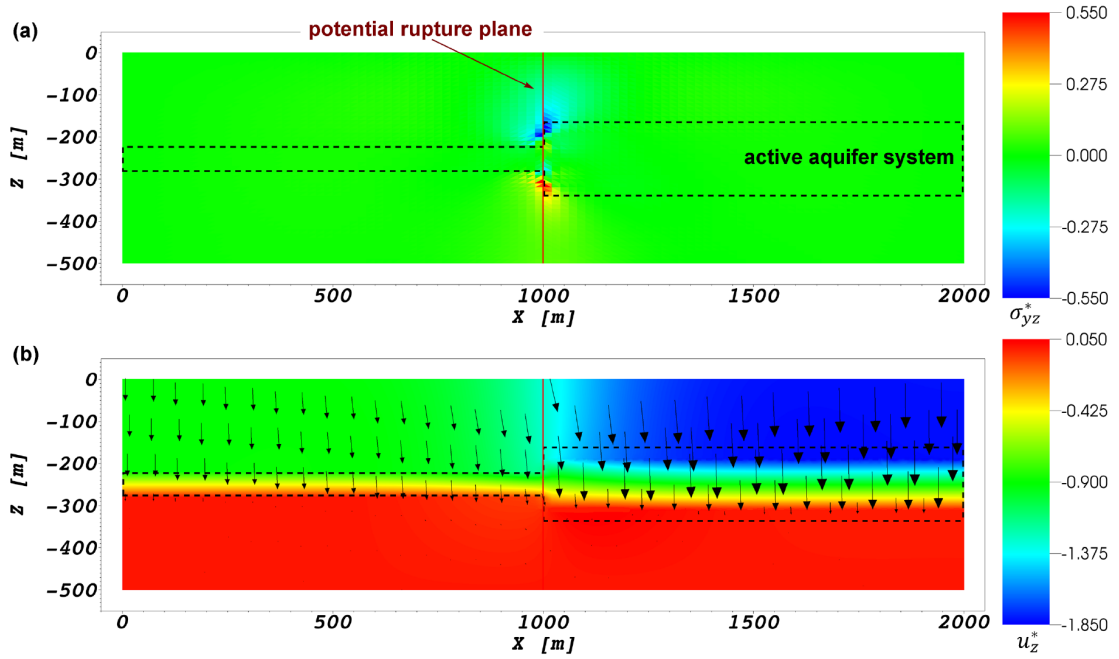

Numerical results

Applications: ground ruptures due to groundwater pumping

- ✓ Buried ridges create stress concentrations on the rock tip and on its vertical projection on the ground
- ✓ Ruptures typically propagate from the land surface downward

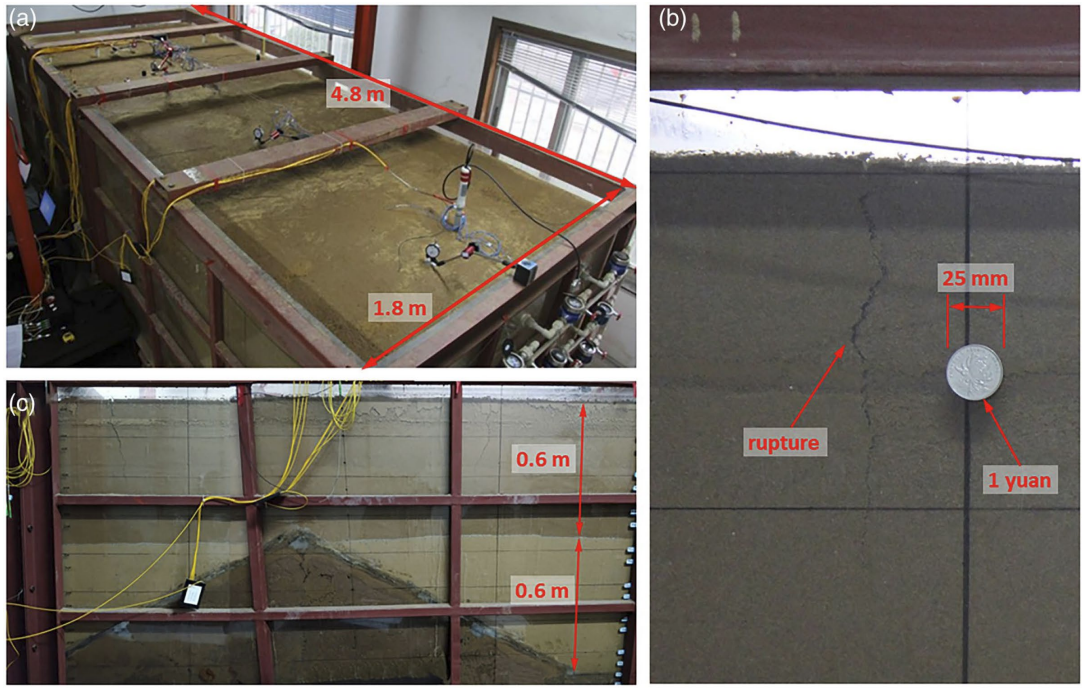

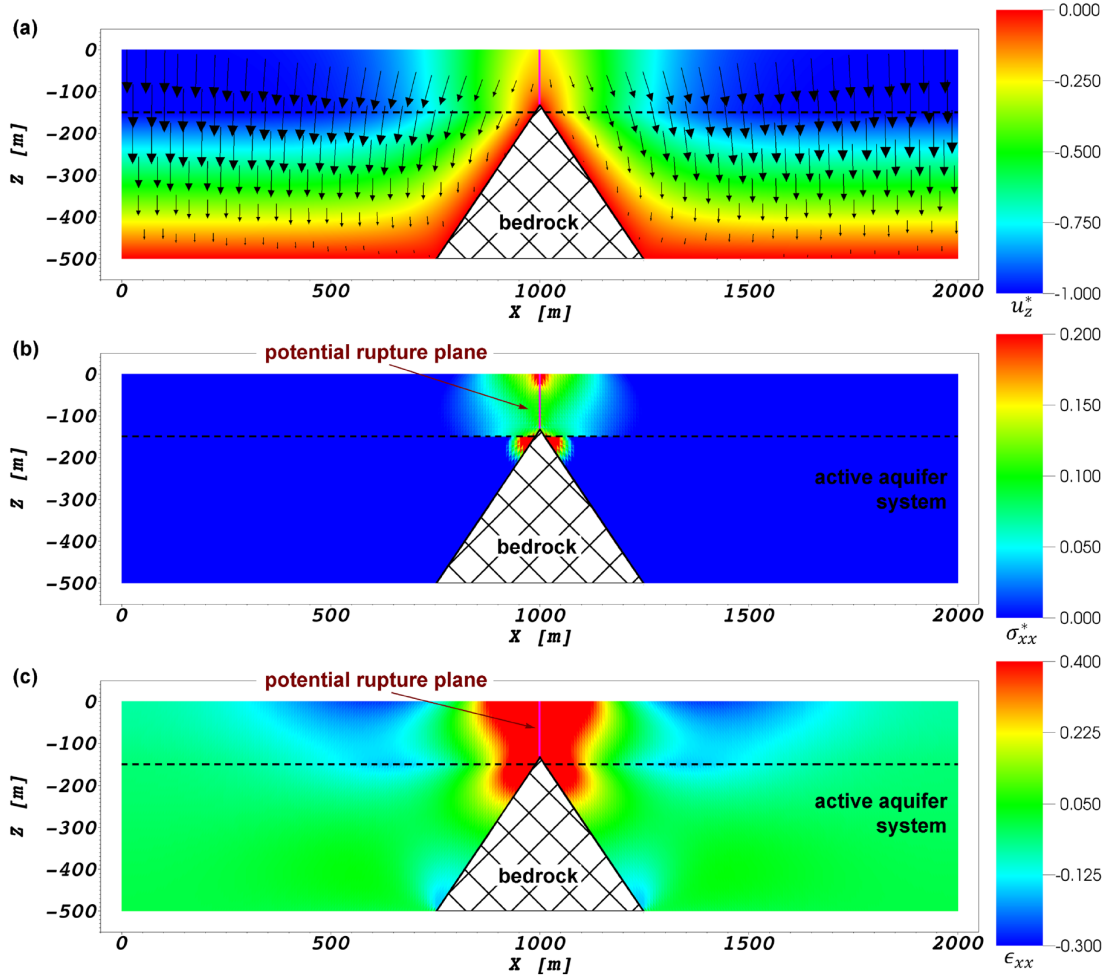

Numerical results

Applications: ground ruptures due to groundwater pumping

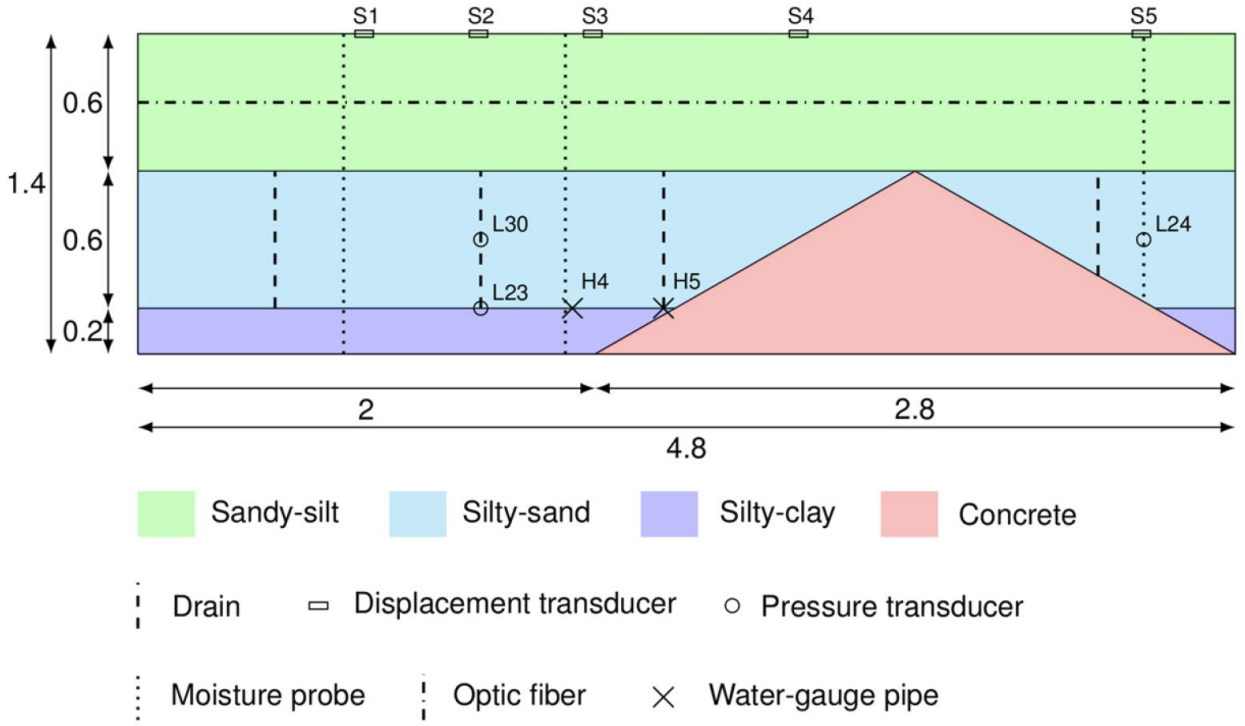

Horizontal and vertical displacements

✓ Lab experiment setup and numerical results

Water saturation

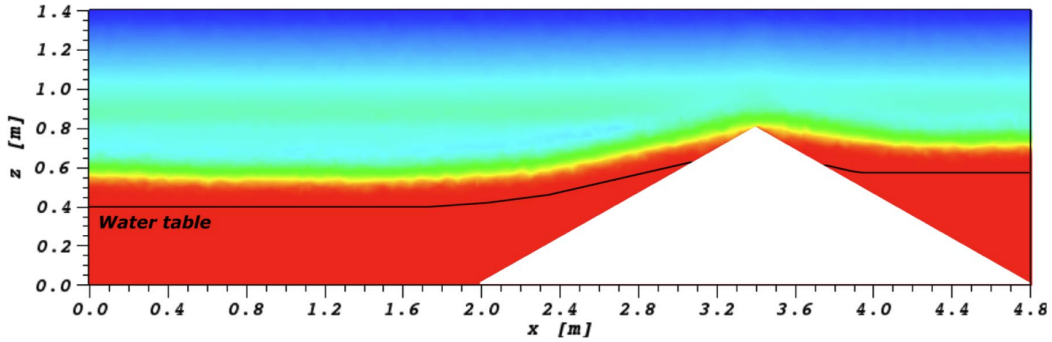

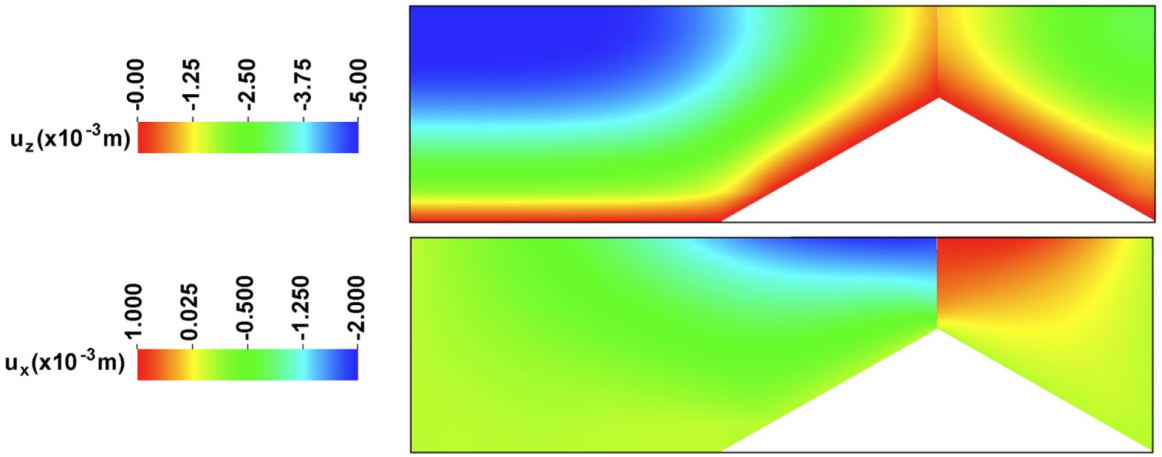

Numerical results

Applications: fault activation in UGS activities

- ✓ The interest in developing UGS projects is continuously increasing worldwide → about 300 UGS sites in Europe, more than 400 UGS sites in the US
- ✓ Geohazards possibly associated with UGS activities:
  - Formation integrity
  - Leakage from the reservoir
  - Land motion
  - Induced and/or triggered seismic events
- ✓ Coping with such issues is necessary for health and safety as related to public perception, economic risk and environmental impact

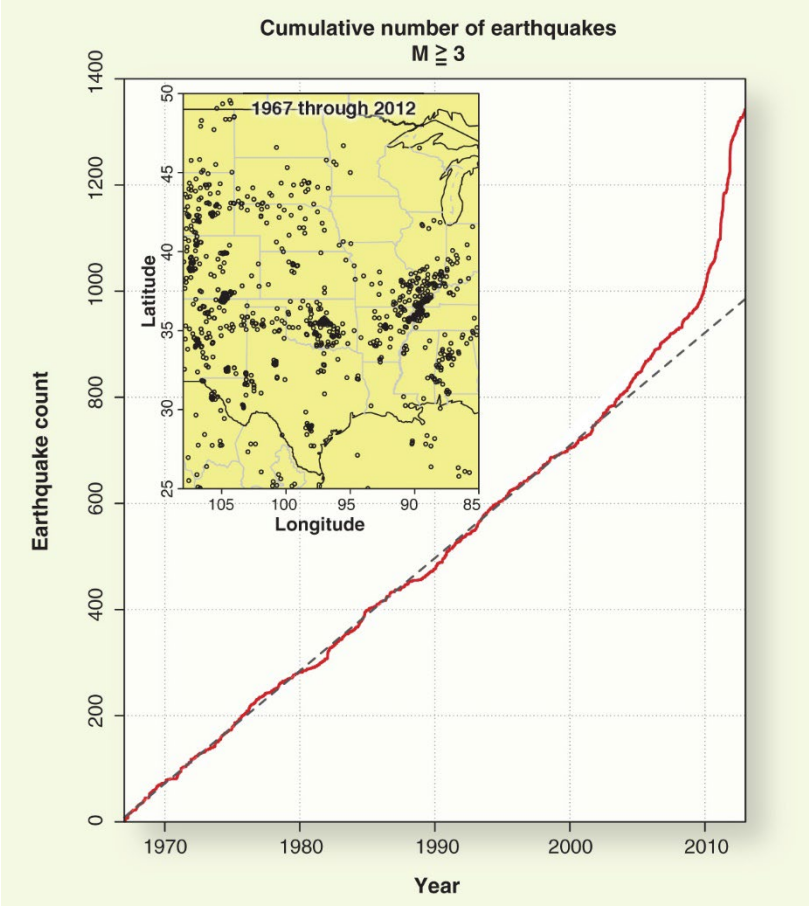

from Ellsworth (Science, 2013)

Numerical results

Applications: fault activation in UGS activities

- ✓ Cases of seismic activity have been recently recorded in a few UGS plants located in the Rotliegend formation, The Netherlands:
  - Primary Production
  - Cushion Gas injection
  - Storage activities

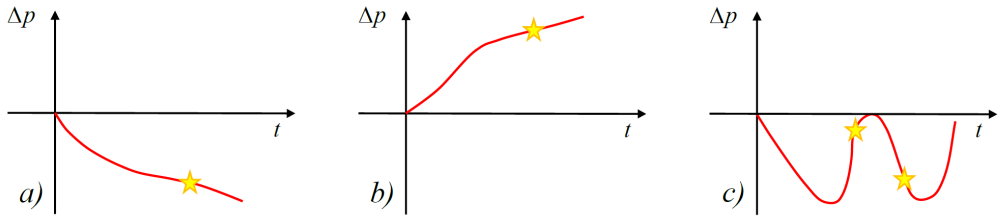

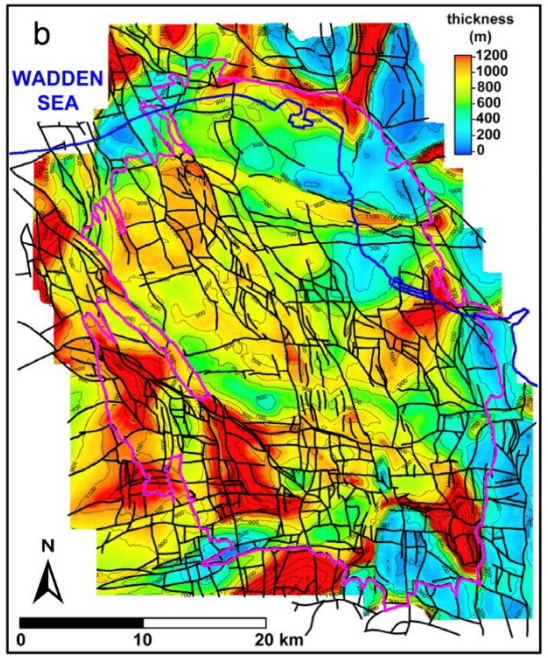

- ✓ The Roetliegend formation spans a depth range between 2000 and 4700 m and is characterized by highly compartmentalized and fractured reservoirs in stiff sandstone rocks overlain by salt deposits (the Zechstein formation)
- ✓ Our aim is to develop mathematical and numerical models to simulate the possible inception of fault motion also in «unexpected» configurations

Numerical results

Applications: fault activation in UGS activities

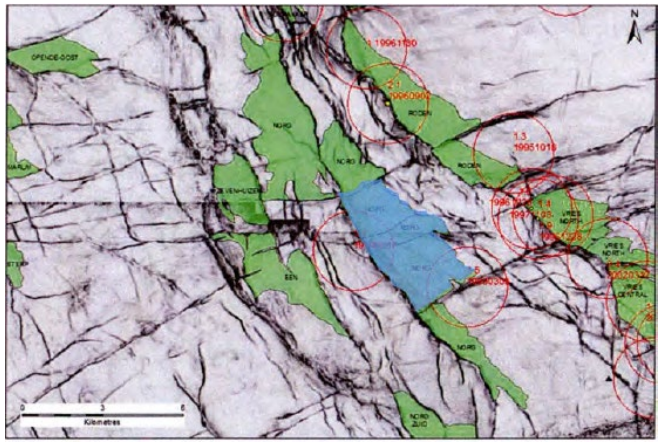

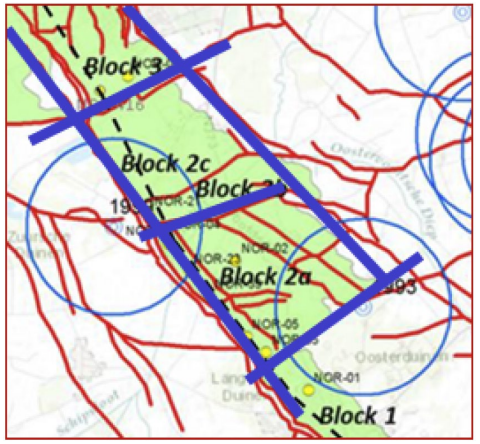

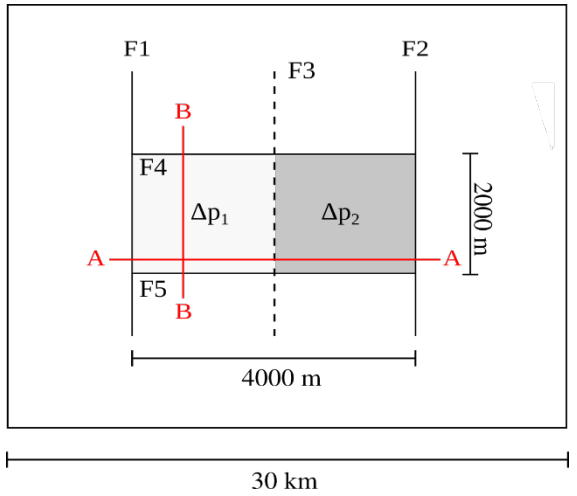

- ✓ Schematic geometry representative of the typical configuration of Ducth UGS fields:
  - Independent blocks with different pressures
  - Bounding vertical and sub-vertical faults
  - Viscous salt formations on top

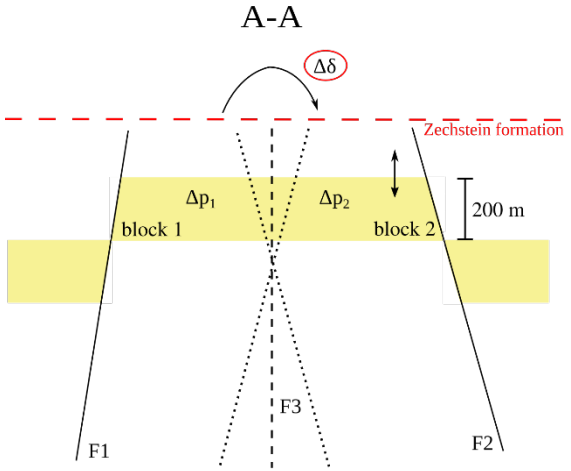

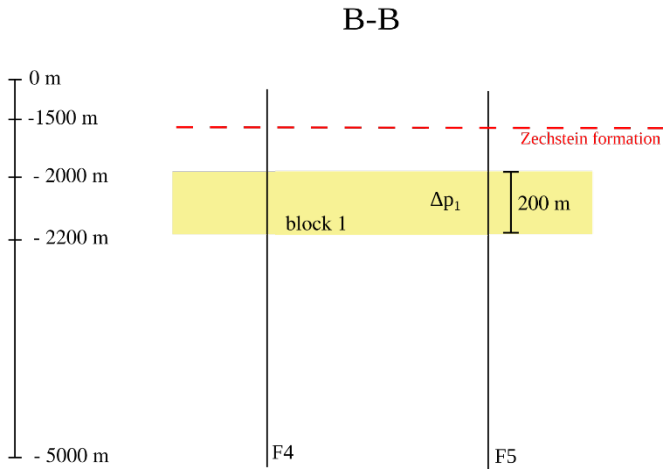

Numerical results

Applications: fault activation in UGS activities

- ✓ Geomechanical parameters typical of the Rotliegend formation
- ✓ Almost isotropic initial stress state (M_1=0.74, M_2=0.83) with principal directions oriented like the bounding faults

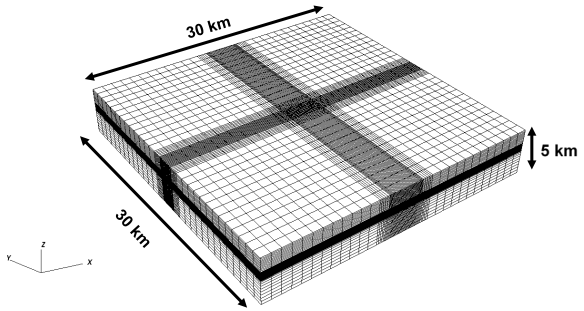

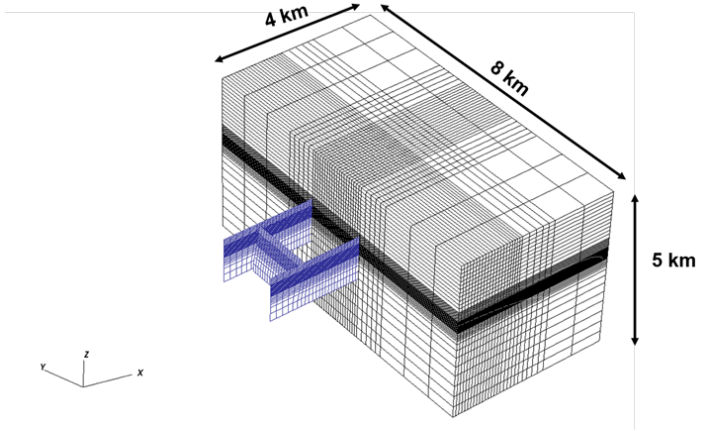

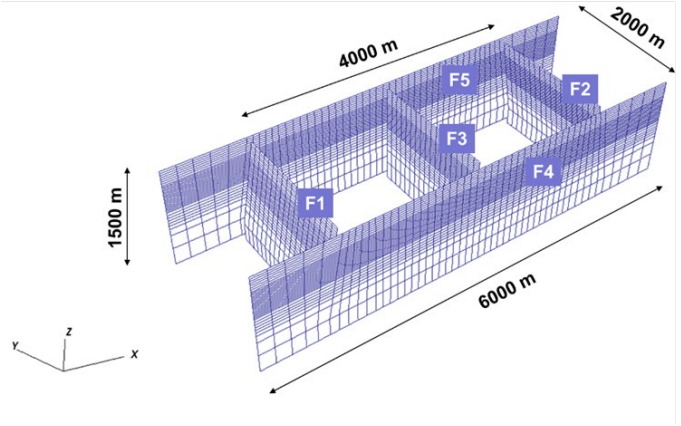

LAYER	DENSITY (kg/m^3)	YOUNG MODULUS (GPa)	POISSON RATIO
Overburden	2200	10.0	0.25
Zechstein Salt	2100	40.0	0.3
Reservoir (Upper Rotliegend)	2400	11.0	0.15
Underburden	2600	30	0.2

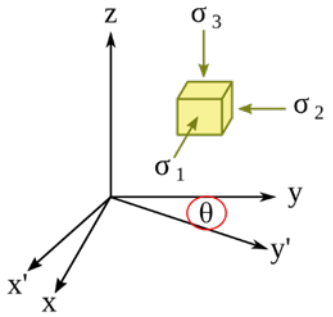

Initial stress regime:

$\sigma_h = \sigma_1 = M_1 * \sigma_3$

$\sigma_H = \sigma_2 = M_2 * \sigma_3$

$\sigma_v = \sigma_3$

Numerical results

Applications: fault activation in UGS activities

- ✓ Micro-seismic activity recorded in gas storage reservoirs in The Netherlands, during both the primary production and the storage phase
- ✓ Computational analysis to investigate the origin and the conditions that can be favorable to occurrences

Norg UGS field

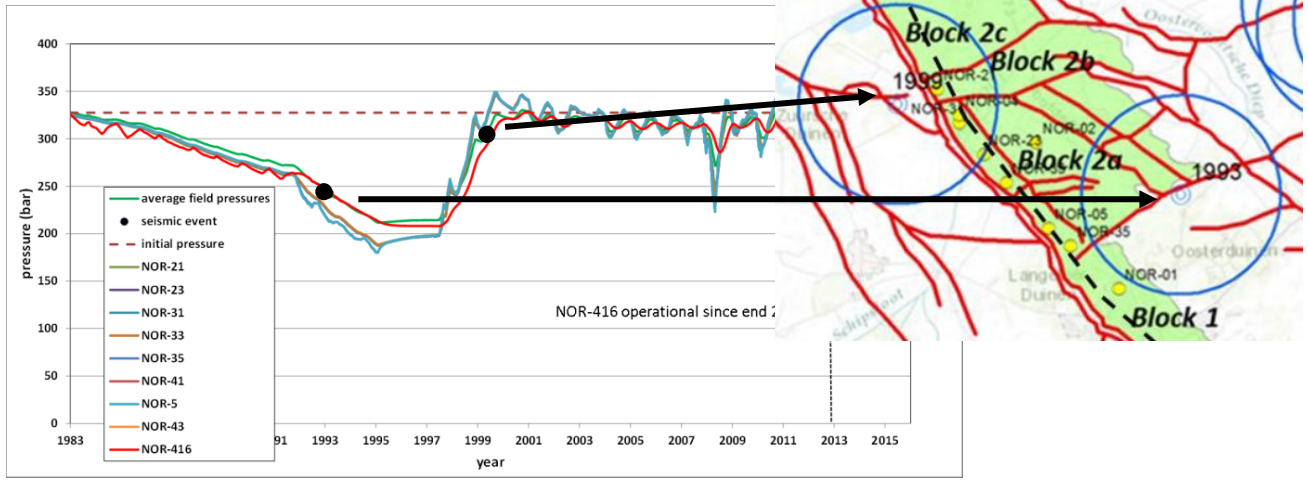

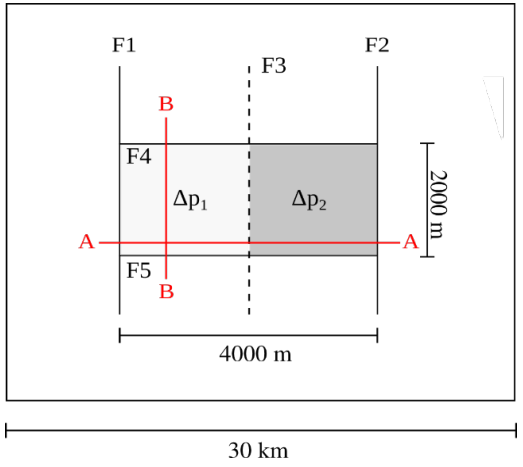

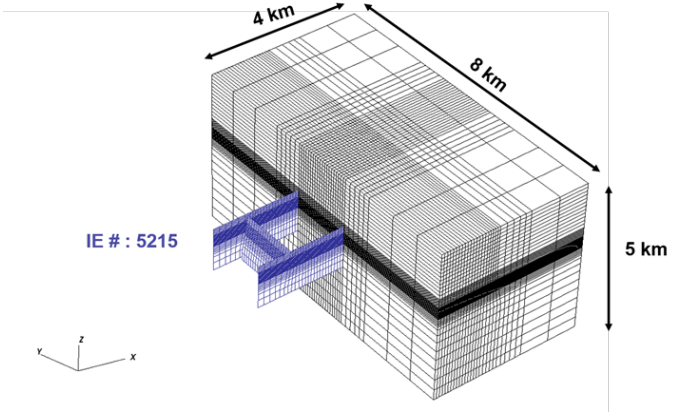

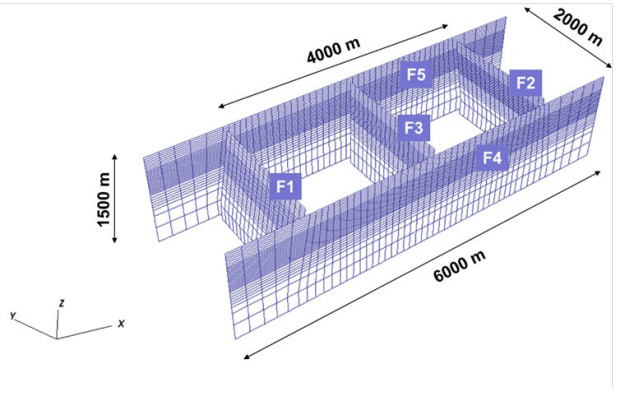

Numerical results

Applications: fault activation in UGS activities

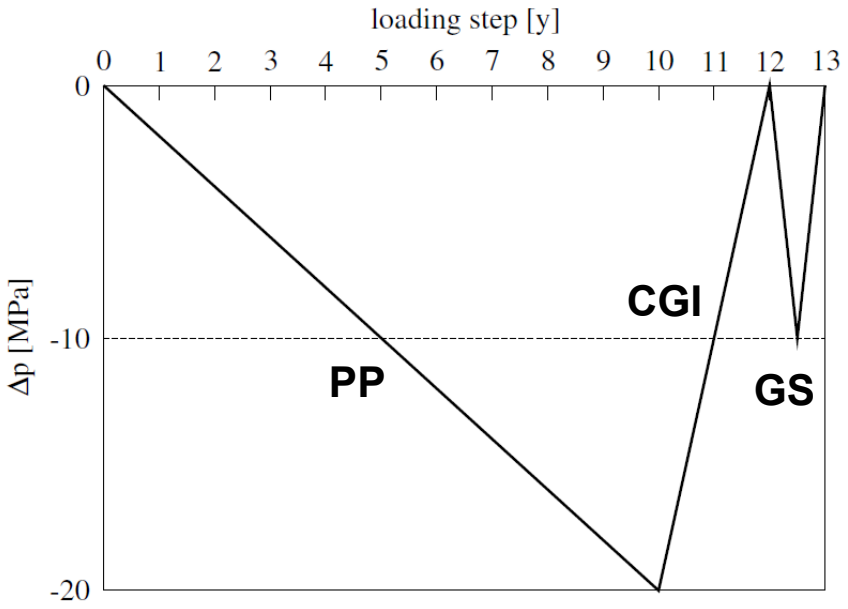

- ✓ The pressure history prescribed in each block of the UGS field includes a Primary Production (PP), Cushion Gas Injection (CGI), and a Gas Storage (GS) stage
- ✓ A loading step corresponds to a 1-year time interval
- ✓ The potential for fault reactivation is measured by the criticality index:

$$\chi = \frac{\|\boldsymbol{t}_T\|_2}{\tau_L} = \frac{\|\boldsymbol{t}_T\|_2}{c - t_N \tan[\varphi(\|\boldsymbol{g}_T\|_2)]}$$

- ✓ A sensitivity analysis on different configuration parameters has been carried out to identify critical situations:
  - Block offset (0-200 m)
  - Central fault dip (-25° - 25°)
  - Reservoir, caprock, and fault properties
  - Biot coefficient (0.6 – 1.0)
  - Initial stress regime ($M_1 = M_2 = 0.4$)
  - Pressure variation (0-200 bar)

Numerical results

Applications: fault activation in UGS activities

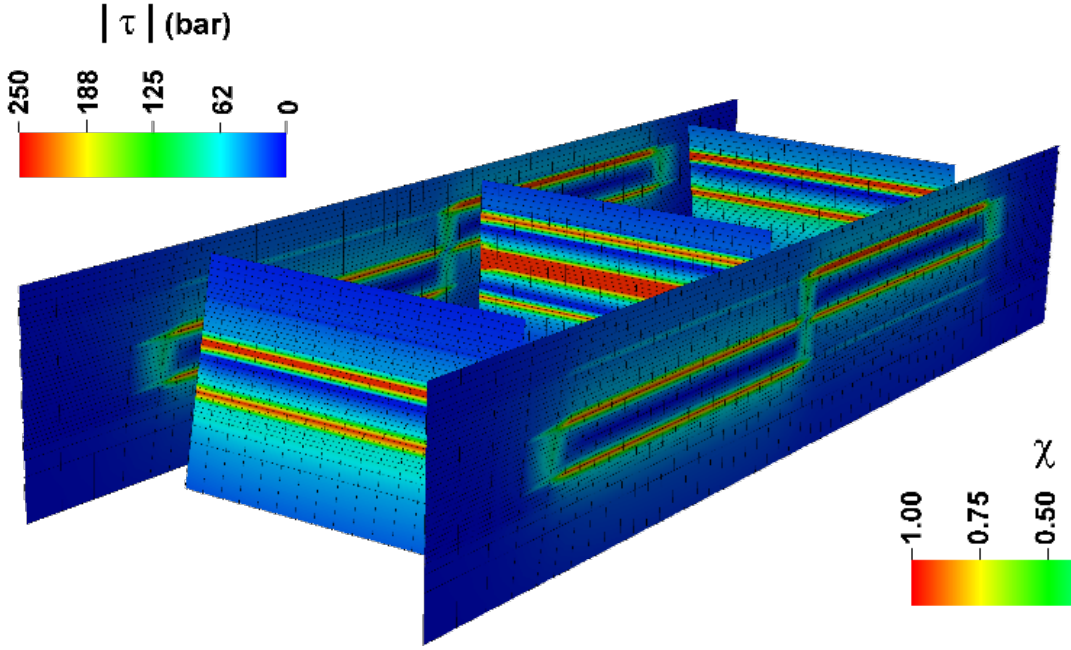

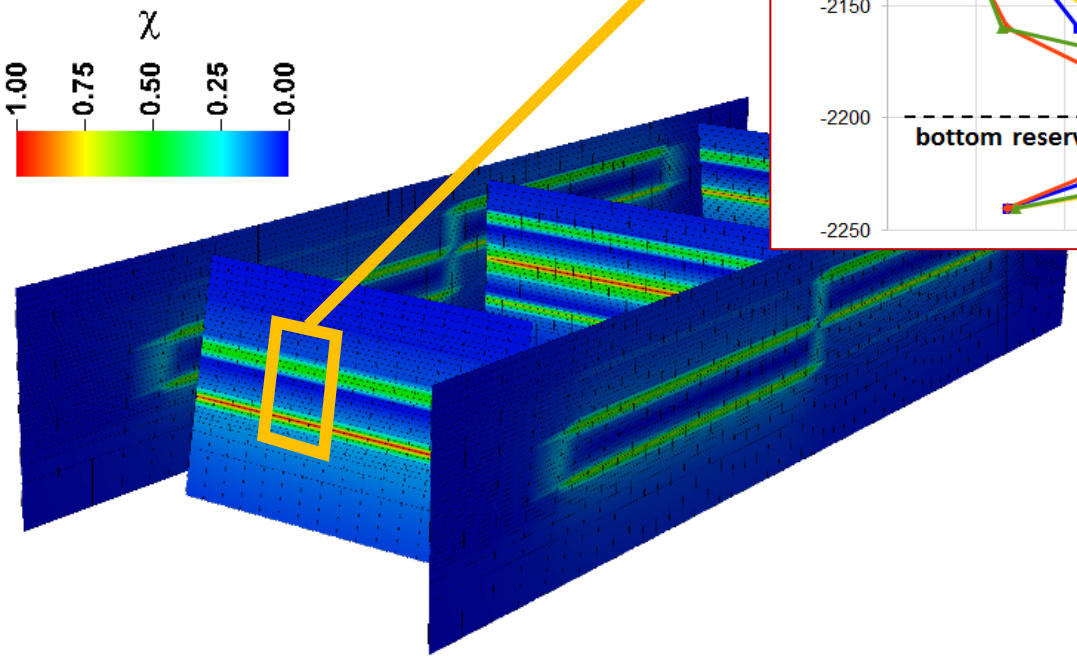

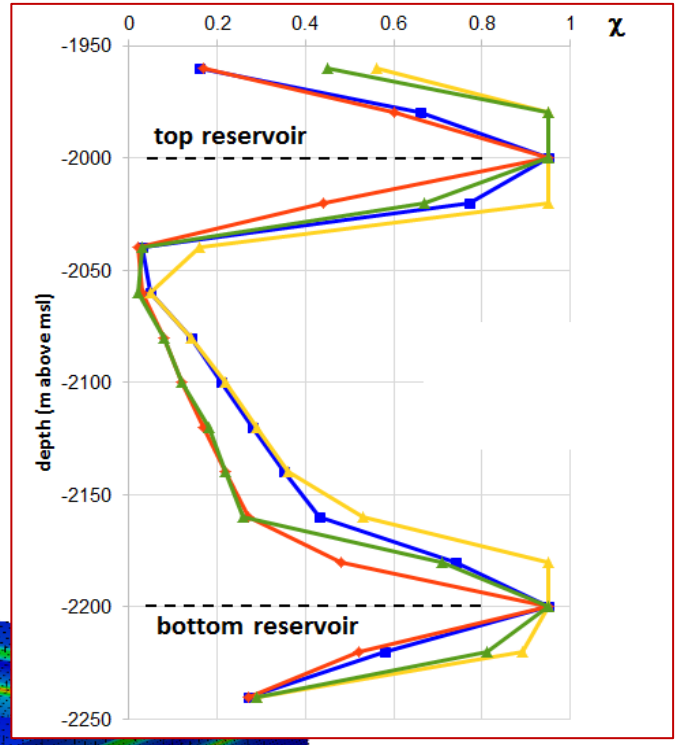

|τ| and χ at the end of primary production

Numerical results

Applications: fault activation in UGS activities

- ✓ Fault activation during primary production leads to a stress redistribution
- ✓ A new (deformed) "equilibrated" configuration that is newly loaded, in the opposite direction, when the pressure variation changes the sign

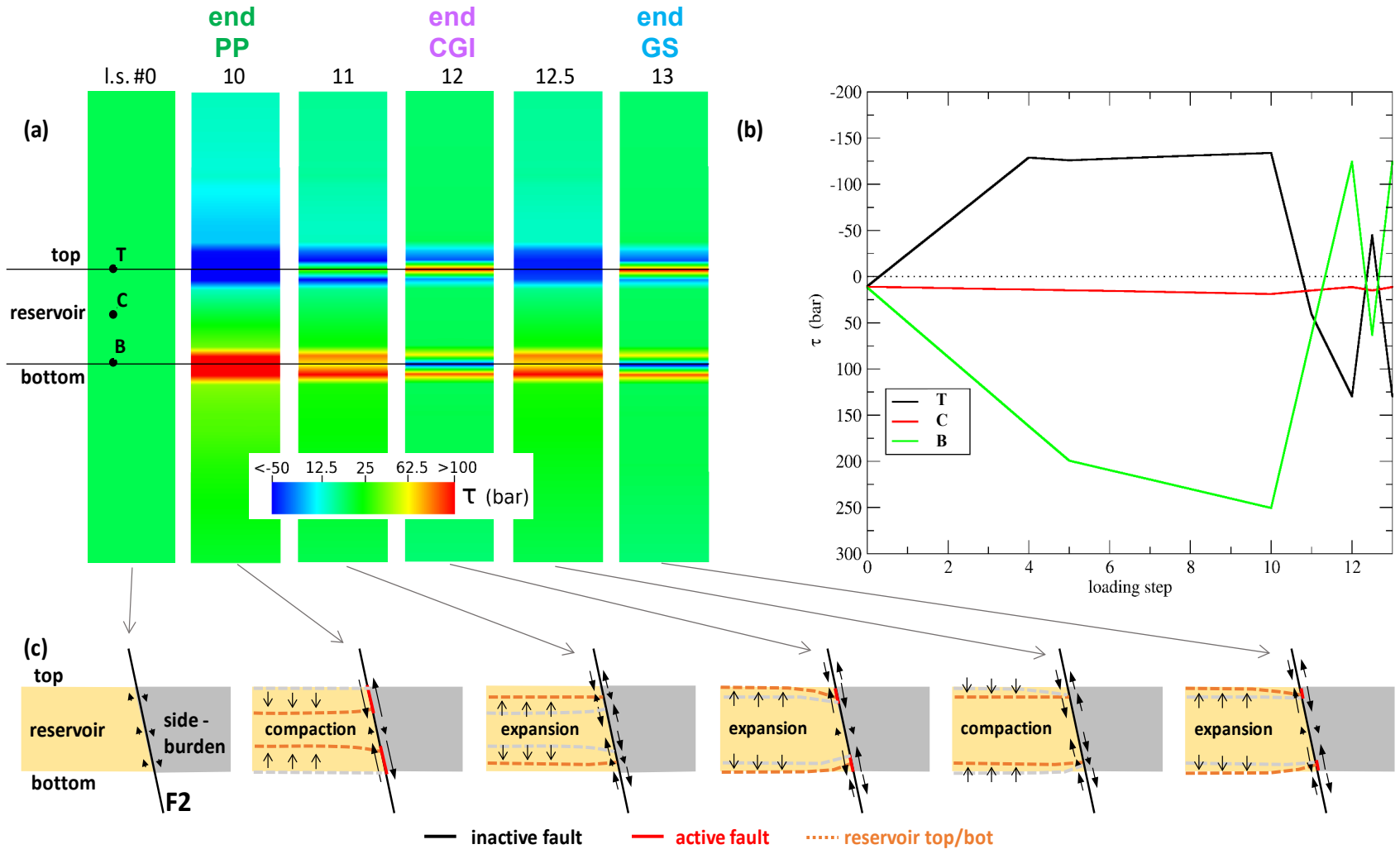

Numerical results

Applications: fault activation in UGS activities

- ✓ A weakening model is implemented to account for the variation of the friction angle from static to dynamic conditions at the fault slipping and a Maxwell model is used to simulate the viscous behavior of the top salt Zechstein formation

$$\begin{cases} \varphi = \varphi_s - \|\boldsymbol{g}_T\|_2 \dfrac{\varphi_s - \varphi_d}{d_c}, & \|\boldsymbol{g}_T\|_2 \le d_c \\ \varphi = \varphi_d, & \|\boldsymbol{g}_T\|_2 > d_c \end{cases} \qquad \dot{\boldsymbol{\varepsilon}}_v = V(\mu)\boldsymbol{\sigma}, \qquad \mu = 10^{17}\ Pa \cdot s$$

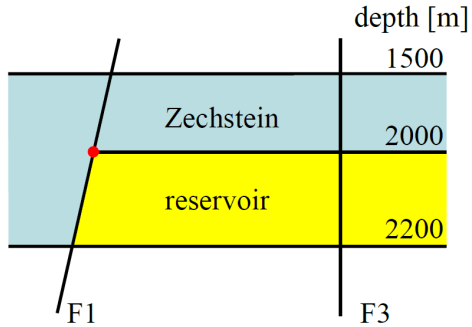

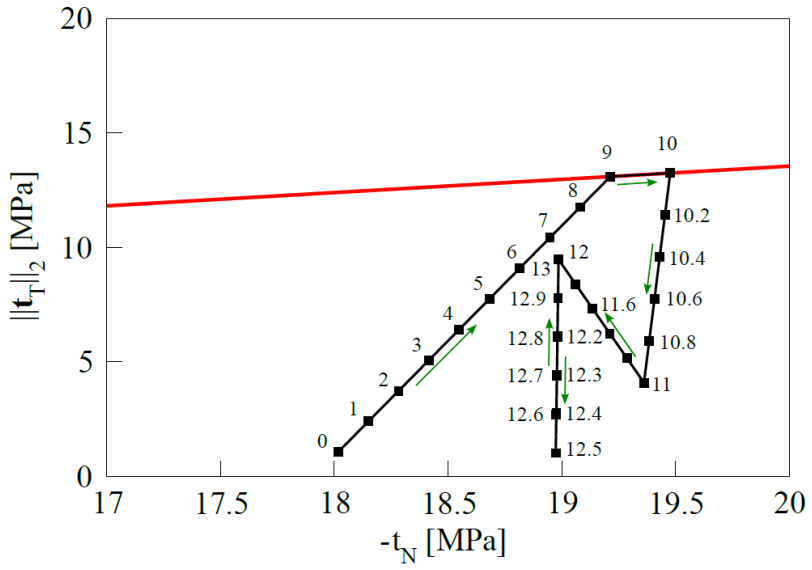

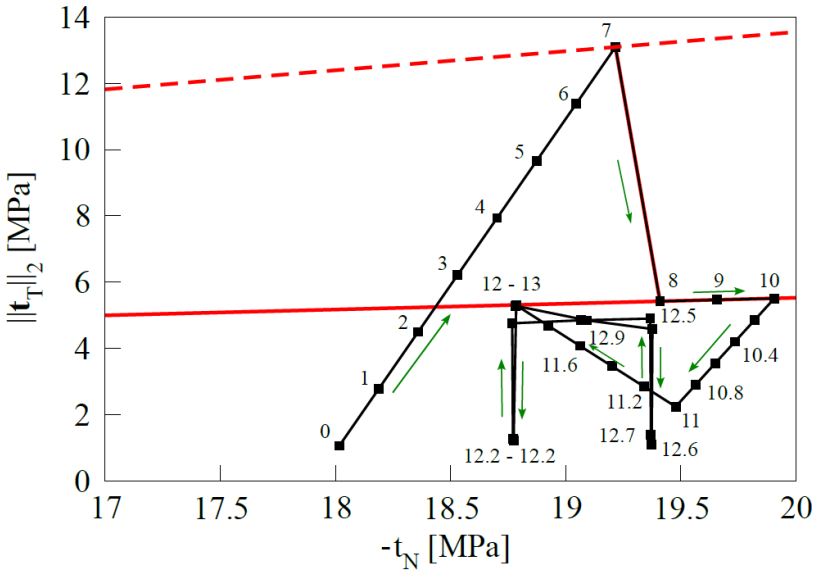

Numerical results

Applications: fault activation in UGS activities

- ✓ The initial stress regime can play a major role: decreasing significantly the horizontal principal components favors an early fault reactivation, with a large area critically stressed and significant sliding
- ✓ Factors increasing the activation risk: (1) a reduced friction angle; (2) an offset between producing blocks; (3) stiffness contrasts between reservoir, caprock, sideburden, and underburden; (4) uneven pressure change in adjacent compartments

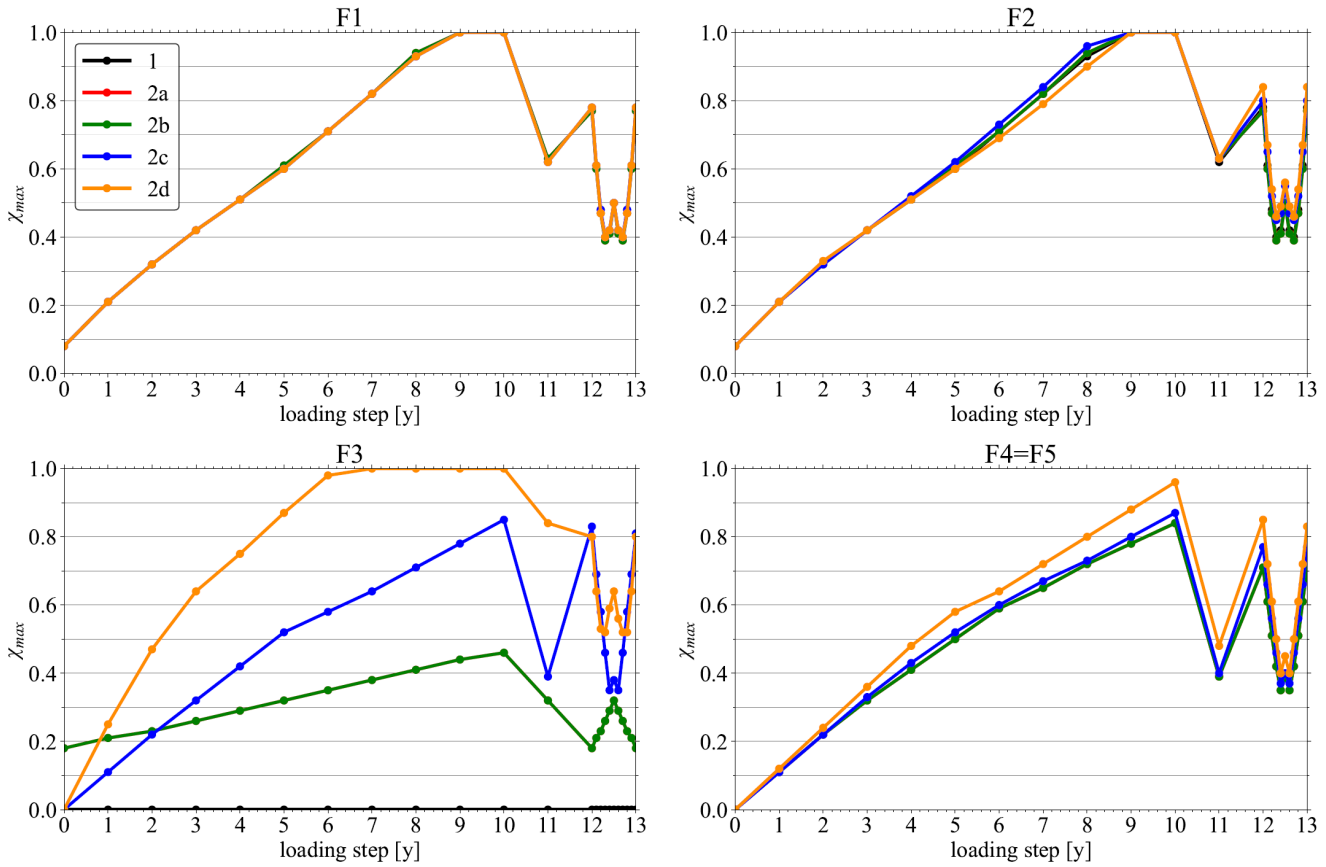

Numerical results

Applications: fault activation in UGS activities

- ✓ Fault reactivation may occur “unexpectedly” during Cushion Gas and Underground Gas Storage stages, following more expected reactivations during Primary Production
- ✓ Activation during Primary Production leads to a stress redistribution and a new "equilibrated" configuration that is re-loaded, in the opposite direction, when the pressure variation changes the sign at the Cushion Gas injection
- ✓ The settings more prone to activation during Primary Production are also the most critical ones during Cashion Gas injection and Underground Gas Storage

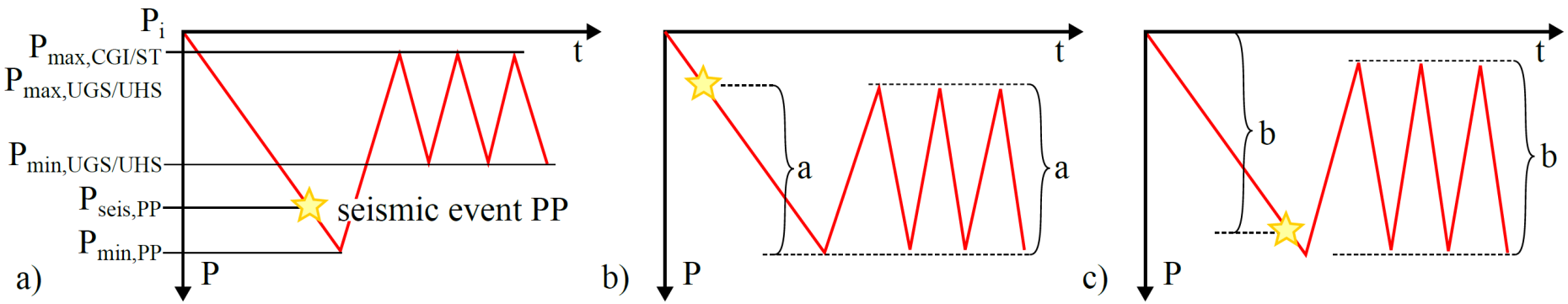

Conclusions

Take-away message and future work

- ✓ **Work objective:** development of a coupled model for the simulation of frictional contact mechanics and fluid flow in fractured porous media
- ✓ **Main characteristics of the proposed approach:** (**1**) low-order Finite Elements for the mechanics, (**2**) Lagrange multipliers to prescribe the contact constraints, (**3**) classical Finite Volume simulation of flow in fractures
- ✓ **Most significant results:**
  - *Introduction of a global stabilization and an active-set strategy to guarantee stability and robustness*
  - *Development of robust, scalable and efficient preconditioning techniques for the inner linear solver*
  - *Successful application to a number of real-world problems: hydraulic fracturing, ground ruptures, fault stability*

Future work

- ✓ Extension to (multi-phase) flow in the porous matrix
- ✓ Parallel implementation with GPU acceleration
- ✓ Application to other storage problems, such as CO2 sequestration and Hydrogen storage

UNIVERSITÀ DEGLI STUDI DI PADOVA

References from the University of Padova group

1. A. Franceschini, C. Zoccarato, S. Baldan, M. Frigo, M. Ferronato, C. Janna, G. Isotton, P. Teatini. *Unexpected fault activation in underground gas storage. Part I: Mathematical model and mechanisms.* Preprint, ArXiV: 2308.02198.
2. A. Franceschini, L. Gazzola, M. Ferronato. *A scalable preconditioning framework for stabilized contact mechanics with hydraulically active fractures*. **Journal of Computational Physics**, 463, 111276, 2022c.
3. A. Franceschini, M. Ferronato, M. Frigo, C. Janna. *A Reverse Augmented Constraint preconditioner for Lagrange multiplier methods in contact mechanics*. **Computer Methods in Applied Mechanics and Engineering**, 325, 114632, 2022b.
4. A. Franceschini, N. Castelletto, J.A. White, H.A. Tchelepi. *Scalable preconditioning for the stabilized contact mechanics problem*. **Journal of Computational Physics**, 459, 111150, 2022a.
5. S. Nardean, M. Ferronato, Y. Zhang, S. Ye, X. Gong, P. Teatini. *Understanding ground rupture due to groundwater over-pumping by a large lab experiment and advanced numerical modeling*. **Water Resources Research**, 57, e2020WR027553, 2021.
6. A. Franceschini, N. Castelletto, J.A. White, H.A. Tchelepi. *Algebraically stabilized Lagrange multiplier method for frictional contact mechanics with hydraulically active fractures*. **Computer Methods for Applied Mechanics and Engineering**, 368, 113161, 2020.
7. M. Frigo, M. Ferronato, Z. Yang, S. Ye, D. Galloway, D. Carreon-Freyre, P. Teatini. *A parametric numerical analysis of factors controlling ground ruptures due to groundwater pumping*. **Water Resources Research**, 55, pp. 9500-9518, 2019.
8. A. Franceschini, N. Castelletto, M. Ferronato. *Block preconditioning for fault/fracture mechanics saddle-point problems*. **Computer Methods for Applied Mechanics and Engineering**, 344, pp. 376-401, 2019.
9. A. Franceschini, M. Ferronato, C. Janna, P. Teatini. *A novel Lagrangian approach for the stable numerical simulation of fault and fracture mechanics*. **Journal of Computational Physics**, 314, pp. 503-521, 2016.
10. M. Ferronato, G. Gambolati, C. Janna, P. Teatini. *Numerical modelling of regional faults in land subsidence prediction above gas/oil reservoirs.* **International Journal for Numerical and Analyical Methods in Geomechanics**, 32, pp. 633-657, 2008.

Other references

1. B.T. Aagaard, M.G. Knepley, C.A. Williams. *A domain decomposition approach to implementing fault slip in finite-element models of quasi-static and dynamic crustal deformation*. **Journal of Geophysical Research - Solid Earth**, 118, pp. 3059-3079, 2013.
2. G. Beer. *An isoparametric joint/interface element for finite element analysis*. **International Journal for Numerical Methods in Engineering**, 21, pp. 585-600, 1985.
3. M. Benzi, G.H. Golub, J. Liesen. *Numerical solution of saddle point problems.* **Acta Numerica**, 14, pp. 1–137, 2005.
4. N. Castelletto, J.A. White, M. Ferronato. *Scalable algorithms for three-field mixed finite element coupled poromechanics.* **Journal of Computational Physics**, 327, pp. 894-918, 2016.
5. S. Cescotto, R. Charlier. *Frictional contact finite elements based on mixed variational principles*. **International Journal for Numerical Methods in Engineering**, 36, pp. 1681-1701, 1993.
6. H. Elman, D.J. Silvester, A. Wathen. **Finite Elements and Fast Iterative Solvers: With Applications in Incompressible Fluid Dynamics.** Oxford University Press, 2014.
7. T.A. Garipov, M. Karimi-Fard, H.A. Tchelepi. *Discrete fracture model for coupled flow and geomechanics.* **Computational Geosciences**, 20, pp. 149-160, 2016.
8. G. Isotton, M. Frigo, N. Spiezia, C. Janna. *Chronos: A general purpose classical AMG solver for High Performance Computing.* **SIAM Journal on Scientific Computing**, 43, pp. C335–C357, 2021.
9. B. Jha, R. Juanes. *Coupled multiphase flow and poromechanics: a computational model of pore pressure effects on fault slip and earthquake triggering.* **Water Resources Research**, 50, pp. 3776-3808, 2014.
10. R. Juanes, J. Samper, J. Molinero. *A general and efficient formulation of fractures and boundary conditions in the finite element method.* **International Journal for Numerical Methods in Engineering**, 54, pp. 1751-1774, 2002.

Other references

11. M.F. Murphy, G. Golub, A.J. Wathen. *A note on preconditioning for indefinite linear systems*. **SIAM Journal on Scientific Computing**, 21, pp. 1969-1972, 2000.
12. J. Rutqvist, J.T. Birkholzer, C.F. Tsang. *Coupled reservoir-geomechanical analysis of the potential for tensile and shear failure associated with CO2 injection in multilayered reservoir-caprock systems.* **International Journal of Rock Mechanics and Mining Sciences**, 45, pp. 132-143, 2008.
13. B. Wohlmuth. *Variationally consistent discretization schemes and numerical algorithms for contact problems.* **Acta Numerica**, 20, pp. 569-734, 2011.

People from the MANGO group


Massimiliano Ferronato


Pietro Teatini


Carlo Janna


Andrea Franceschini


Claudia Zoccarato

Faculty staff


Caterina Millevoi

Post-Doc


Selena Baldan


Daniele Moretto


Urooj Qayyum

PhD students


Giovanni Isotton


Matteo Frigo


Stefano Nardean


Laura Gazzola

Former collaborators

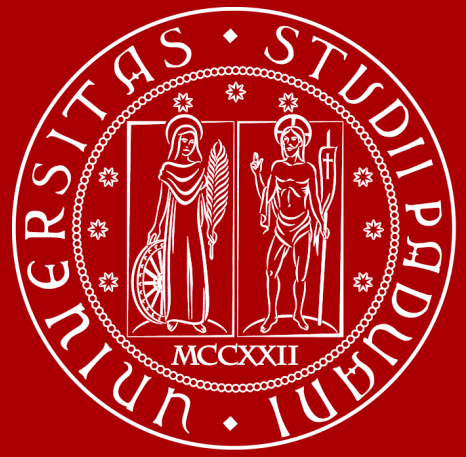

UNIVERSITÀ
DEGLI STUDI
DI PADOVA

Thanks for attending!

Questions?

Massimiliano Ferronato: *Massimiliano.ferronato@unipd.it*